Advanced Geologic Characterization in Support of Class VI Injection Permit

1.0 Introduction

Geologic sequestration of carbon dioxide in the United States is regulated by the Environmental Protection Agency via the Class VI injection permit. As part of the permitting process, a detailed characterization *o*f the injection and confining zones is required in order to ensure that the injected CO2 will remain permanently sequestered in the subsurface. For typical hydrocarbon extraction, derivation of bulk petrophysical properties is adequate to predict hydrocarbon recovery rates. However, for sequestration purposes, it is necessary to conduct detailed geologic analysis due to the buoyant nature of CO2 and in order to account for sequestration in each of the four primary CO_2 trapping mechanisms in the subsurface: structural, residual, solubility, and mineralogical.

This paper documents the advanced characterization techniques implemented at a sequestration site in Wellington, Kansas in support of a Class VI injection permit (Figure 1). The 5,000 feet deep and 1,000 ft thick Arbuckle Group of Cambro-Ordovician age is being considered as a suitable site for large scale Carbon Capture and Storage (CSS). To facilitate this endeavor, the U.S. Department of Energy funded a multi-year study to characterize the aquifer and the overlying confining zone specifically for CO_2 sequestration purposes. Two 5,000+ feet wells, KGS 1-28 and KGS 1-32 (Figure 1) were drilled to basement to derive an extensive suite of geophysical logs, cores, and swab samples, in order to better understand the geology/hydrogeology, derive petrophysical properties, and conduct hydraulic tests. Sedimentary basins throughout the world have been identified for sequestration purposes due to presence of an overlying confining zone that is typically present above carbonate and sandstone formations. The characterization techniques presented in this document can be applied to other sites being considered for geologic sequestration.

The Arbuckle aquifer at the site exists between 4,000 -5,000 ft below ground surface (Figure 2). Shales overlying the Arbuckle Group have caprock characteristics and function as the top confining zone. Precambrian-age basement granites underlie the Arbuckle Group and provide basal confinement. The petrophysical properties governing flow and transport in this injection zone are highly variable due to the presence of complex interbeds of fractured, vuggy dolomite and shale as

reflected in the geophysical logs (Figure 3). The entire process of characterizing the formations and incorporation in a simulation model (which is required by the EPA to make projections about the fate and transport of the sequestered CO_2) consists of the following steps:

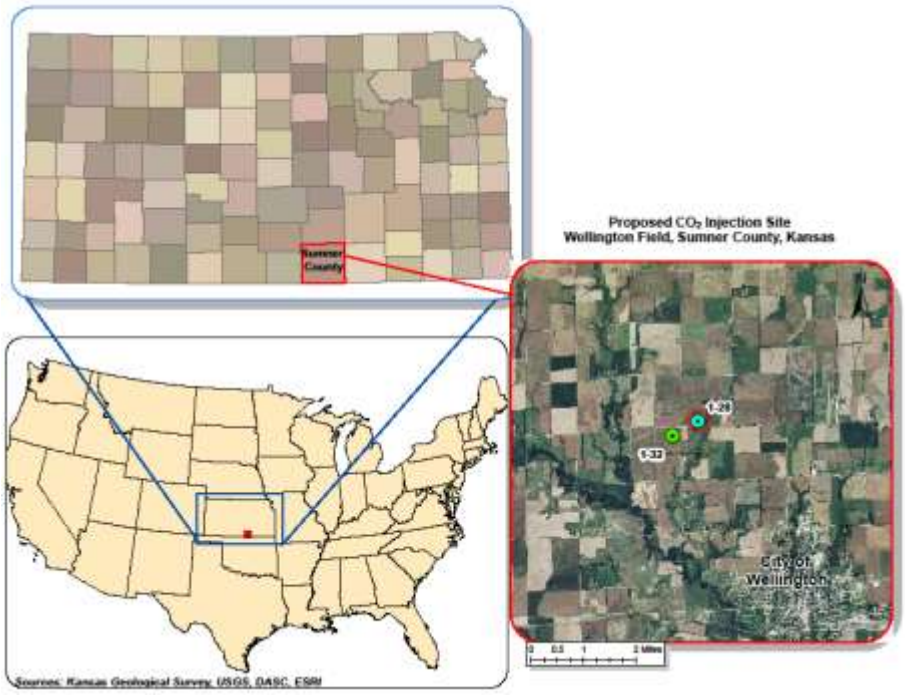

Figure 1 Location of Wellington geologic sequestration site.

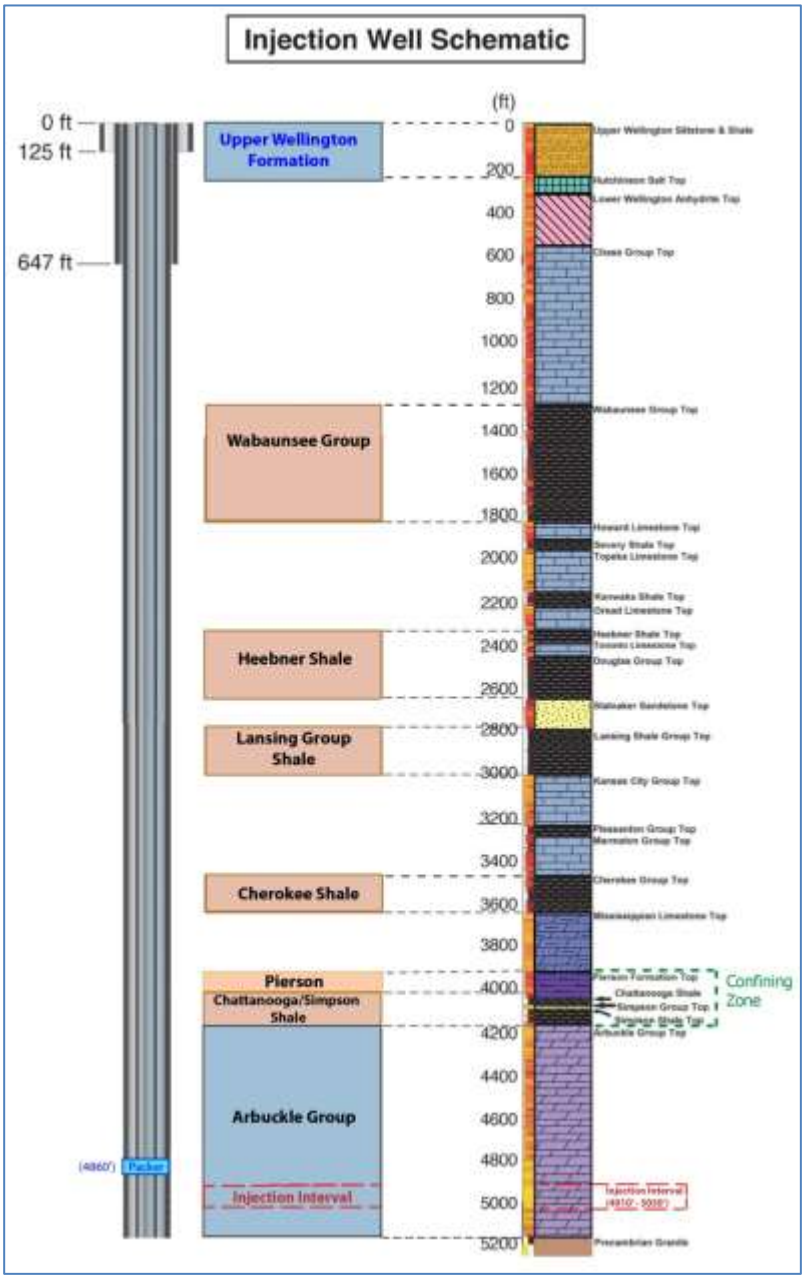

Figure 2 Stratigraphic column at the CO_2 injection well (KGS 1-28).

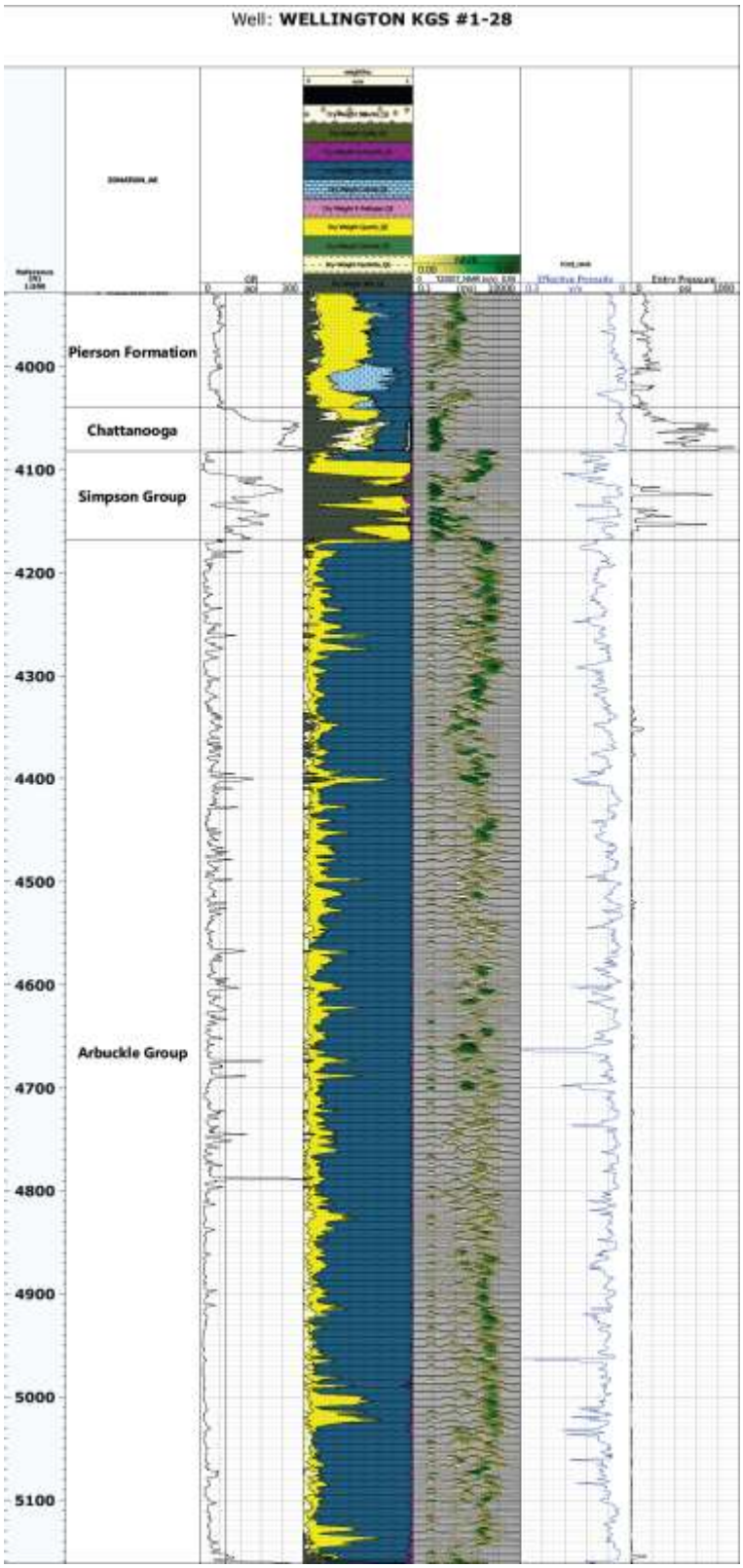

Figure 3 Geologic logs at the injection well site (KGS 1-28).

- Site data acquisition
- Data processing
- Site geologic characterization
- Validation of geologic characterization
- Regional hydrogeologic extrapolation using geomodel
- Upscaling geomodel to reservoir simulation model

2.0 Data Acquisition and Testing

An extensive suite of geophysical logs were obtained and tests conducted at two 5,000+ feet wells drilled to basement (Table 1). The purpose of each log/test and how the data was used to characterize the formation are presented below.

Geophysical Logs
Gamma Ray
Resistivity
Magnetic Resonance Image
Geochemical
Array Compensated True Resistivity
Temperature
Compensated Spectral Gamma Ray
Microlog
Spectral Density Dual Spaced Neutron Log
Annular Hole Volume Log
Extended Range Micro Imager Correlation Plot
Core Samples
Porosity and Permeability
Mineralogy and Soil Characterization
CO_2 Compatibility
Drill Stem Test
Geochemistry
Pressure and Temperature
Swab Samples
Geochemistry and CO_2 Compatibility
Injection Test
Permeability, Head, Fracture Gradient
Seismic Data
Structure and Impedance Mapping

Table 1 Recommended geophysical logs to be acquired and tests to be conducted in support of the Class VI permit.

Array Compensated True Resistivity (ACTR)

ACTR involves obtaining multiple measurements of resistivity which reflects conditions at different distances beyond the borehole wall so that the effects of drilling-mud invasion can be factored out for a reading of the true formation resistivity. The data is used for evaluation of (1) formation water salinity variations and (2) the subdivision of pore volume between electrically connected and unconnected pores, which has important implications for permeability determination.

Temperature

Temperature logs from surface to injection zone are used to specify temperature dependent formation properties (formation brine resistivity, solubility, and phase behavior of CO2) in the numerical model.

Compensated Spectral Natural Gamma Ray

The Compensated Spectral Natural Gamma Ray (CSNGR) log provides insight into the mineral composition of the formations. Measurement of natural gamma-radiation of formations, partitioned between the three most common components of naturally occurring radiation in sandstones and shales (potassium, thorium, and uranium) is used for (1) correlation between wells, so that laterally continuous zones can be identified: (2) shale evaluation, which is particularly important in the evaluation of sealing intervals and baffles: and (3) the recognition of "hot" uranium zones, generally resulting from diagenesis and sometimes indicative of fractures.

Microlog

The Microlog records normal and lateral microresistivity at a much higher vertical resolution than standard resistivity logs, but has less depth of investigation than standard resistivity logs. The data is used to (1) characterize resistivity of thin zones and (2) provide an indication of mudcake buildup as a good diagnostic of permeable zones.

Spectral Density Dual Spaced Neutron Log

This porosity logging suite can be integrated with magnetic resonance imaging (MRI) and neutron-density crossplot (PHND) porosity logs for high grade interpretation of porosity. The photoelectric index (Pe) accompanies modern density logging tools and records the absorption of low-energy

gamma rays by the formation in units of barns per electron. Logged value is a direct function of the aggregate atomic number (Z) of the elements in the formation, and therefore is a sensitive indicator of mineralogy. Pe is combined with neutron porosity, and bulk density information to conduct a Rhomaa-Umma analysis for determination of mineralogy as discussed below.

Annular Hole Volume Log

Used to identify unusual borehole enlargements.

Extended Range Micro Imager Correlation (ERMIC) Plot

The high resolution electrical image of borehole wall provided by the (ERMIC) plot is used for recognition and orientation analysis of (1) fractures, both natural and drilling-induced; (2) vuggy porosity, and (3) shaley zones. A consistency is typically noted between the observations from ERMIC, core, and MRI data. This correlation can be used to extend the delineation of major pore types in the intervals that are not cored.

Magnetic Resonance Image (MRI)

The MRI log measures the relaxation time of hydrogen within the pores exposed to a magnetic field whose spectrum reflects the distribution of pore sizes. The MRI data can be used to obtain a distribution of the pore size, and estimate permeability and porosity values by calibrating to core measurements. The MRI log is also used to determine the sealing potential of caprock by deriving CO2 entry pressure estimates in the confining zone as discussed below.

Radial Cement Bond Log (RCBL)

RCBL tool captures downhole data that ensures reliable cement bond evaluation. The tool is equipped with one omni-directional transmitter, and two omni-directional receivers, as well as eight radial receivers for comprehensive borehole coverage. An inspection of the log will assist in ensuring that there is a competent cement bond in the well, and the absence of any vertical channels through which pressurized fluids could migrate upward into overlying/underlying formations.

Helical Computerized Tomography (CT) Scan

CT scans are used to evaluate the texture of the rocks and to inspect for the presence of very minute fractures in the confining zone.

Sonic Log

The acoustic measurement of porosity records the first arrival of ultrasonic compressional waves and is primarily sensitive to interparticle porosity that occurs between grains or crystals within carbonates and is often referred to as “primary” or “matrix porosity”. In contrast, the MRI, neutron, and density measurements respond to pore spaces at all scales and so provide a measure of total porosity. The difference between the acoustic porosity and the total porosity is termed the “secondary porosity” which can be interpreted to be vuggy porosity, where vugs can range in size anywhere from a dissolved grain to large cavities. The overlay of the MRI porosity with the acoustic (sonic) porosity typically suggests “vuggy facies” in the carbonate injection zone and tighter (less complex) “matrix facies” in the baffle zones within the carbonate injection zone.

Geochemical Logs

Geochemical logs are used to characterize elemental composition and mineralogy and assist in evaluating reaction rates in the presence of free phase CO2.

Core Samples

Core samples were obtained at KGS 1-32 within a 1600 feet interval spanning from the bottom of the Arbuckle into the Cherokee Shale above the Mississippian System. The samples were used for thin-section spectroscopy, geochemical analyses, lab based derivation of permeability of porosity estimates, and fracture investigations.

Drill Stem Test (DST)

DST’s were conducted at various intervals to obtain the ambient pressures, obtain geochemical samples, and derive estimates of formation permeability.

Pressure Pulse or Injection Test

These tests assist in obtaining permeability estimates in the injection zone and can be used to supplement the permeability estimates derived from DST’s. Additionally, the data is useful for model calibration and to identify faults in the study area.

Swab Samples

Formation waters were collected during Drill Stem Tests and swab sampling. The samples were analyzed to establish baseline geochemical conditions and salinity distribution throughout the Arbuckle injection zone. Various geochemical studies were conducted in order to validate the geologic characterization derived from core and log studies.

3.0 Formation characterization at site of acquired logs

3.1 Effective Porosity

The Arbuckle is a triple-porosity system of interparticle, fracture, and vuggy pores. Typically, fracture porosity in carbonates is small in volume (1 to 2%) and so difficult to discriminate, as contrasted with vuggy porosity. Vugs can be either connected or isolated. The effective porosity was estimated by collectively using the MRI, sonic, and the resistivity logs.

The MRI (magnetic resonance imaging) log is lithology-independent and its porosity curve reflects the total pore containing both moveable fluids and capillary-bound water. The MRI tool contains a powerful magnet that realigns the axes of hydrogen nuclei within the rock fluids and then allows them to relax to their natural configuration. The relaxation times correspond to the interaction between the hydrogen nuclei and the pore walls, with the result that relaxation times are mainly controlled by the amount of internal surface area of the rock porosity network. Smaller pores are recorded as short T2 relaxation times and larger pores as longer relaxation times. The log subdivides the relaxation time scale into bins and the MRI log porosity is then the sum of binned porosities measured at different T2 relaxation times. Very slow T2 times reflect pores that would correspond to vugs observable in visual examination of core. The T2 distribution can therefore be subdivided between pores with moveable fluids and pores with bound water, using a cut-off that is known to be variable in carbonates, but often chosen at about 100 ms. Evidence of the ability of the MRI log to discriminate vugs is provided by Figure 4, where the degree of vugginess observed from core examination of the entire Arbuckle is matched with “megaporosity” from the MRI log as the summed porosities with T2 relaxation times of greater than one second. Notice the vug zones in the upper and lower portions of the Arbuckle. Conceptually therefore, the middle of the Arbuckle is referred to as the Baffle Zone.

The acoustic (sonic) measurement of porosity records the first arrival of ultrasonic compressional waves and is primarily sensitive to interparticle porosity that occurs between grains or crystals within carbonates and is often referred to as “primary” or “matrix porosity”. The difference between the acoustic porosity and the total porosity is termed the “secondary porosity” which is interpreted to be vuggy porosity, where vugs can range in size anywhere from a dissolved grain to large cavities. Connected and unconnected vugs can be identified by using the resistivity log. Resistivity log values are controlled by the formation water resistivity and the volume of pore space. Pores that form isolated dead space are bypassed and so do not contribute to the conductivity of the rock.

When the three estimates of porosity (MRI, acoustic, and resistivity) are assessed together, the total pore space can be subdivided between interparticle and vug (MRI minus acoustic porosity) and the vug porosity further subdivided between connected and non-connected vugs. The volume of connected vugs corresponds to the resistivity porosity minus the sonic porosity; the volume of non-connected vugs is the MRI porosity minus the resistivity porosity. This threefold porosity partition is shown in Figure 5 for the injection zone in the lower Arbuckle.

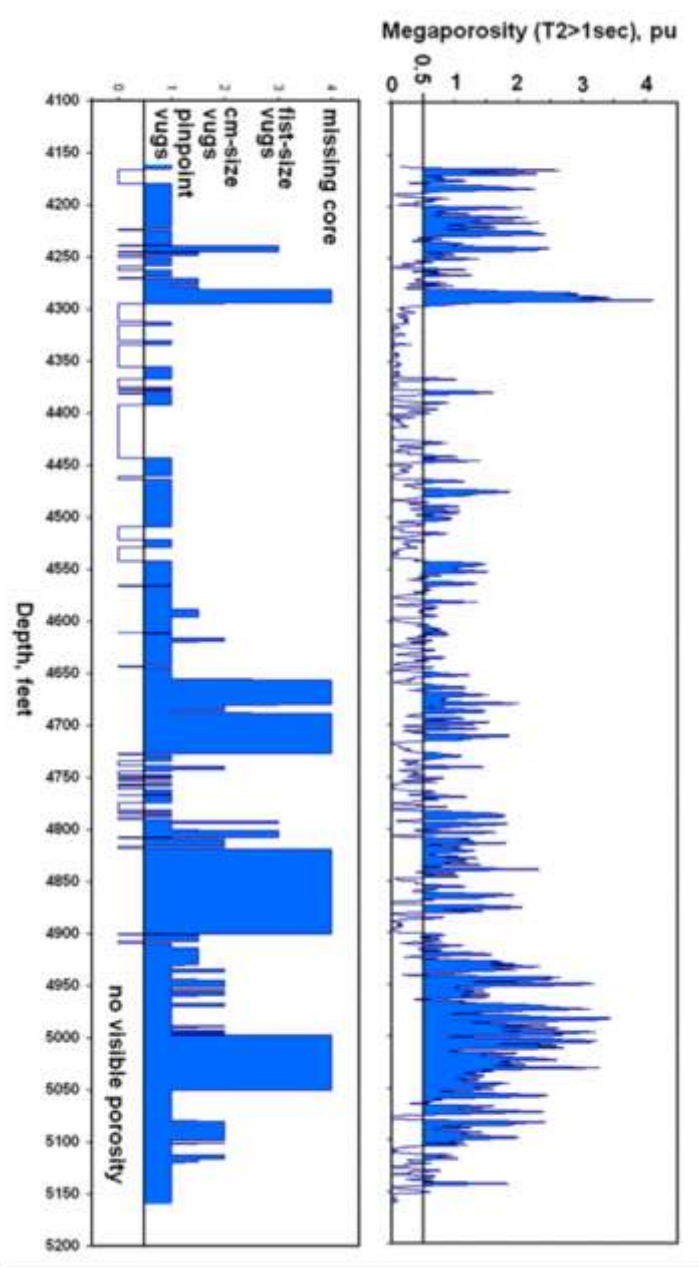

Figure 4 Visual observation of vugs from core in the Arbuckle of KGS 1-32 (left) compared with summed porosities of the MRI log with T2 relaxation times greater than one second (right).

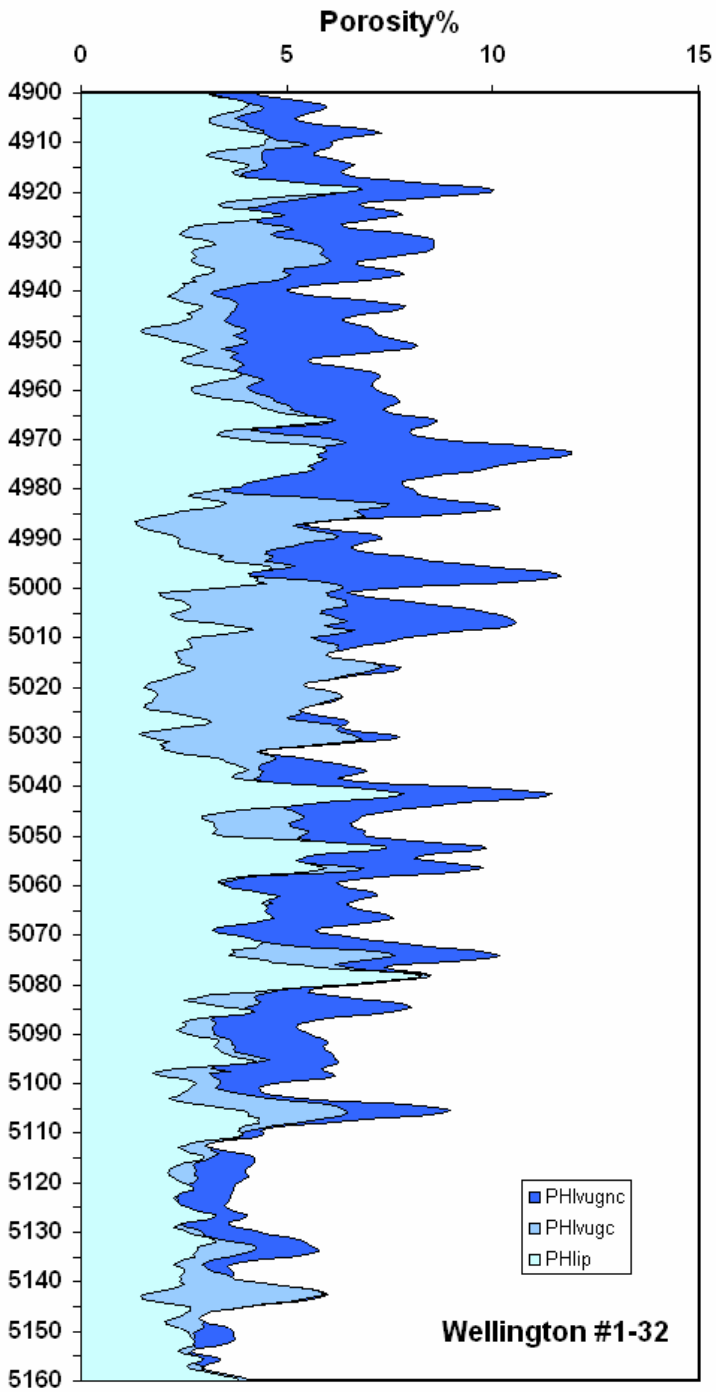

Figure 5 Subdivision of MRI effective porosity within the injection zone (lower Arbuckle) into interparticle porosity (PHIip), connected vugs (PHIvugc), non-connected vugs (PHIvugnc) by sonic and resistivity log partitioning.

3.2 Permeability

The Flow Zone Indicator (FZI) method for assigning hydraulic flow units (Amaefule, 1993) is recognized as one of the best technique available for reservoir characterization. It is based on the well-known Kozeny-Carman (1927) equation for estimating hydraulic permeability (in milliDarcy);

$$K = 1014 \left[\frac{1}{F_s \tau^2 S_{gv}^2}\right] \quad \frac{\phi_e^3}{(1-\phi_e)^2}$$

Where, F_s represents the Shape factor, τ the tortuosity, S_{gv} the surface area per grain volume, and ϕ_e the effective porosity,

The square root of the term, $\left[\frac{1}{F_s \tau^2 S_{gv}^2}\right]$, was referred to by Amaefule et al. as the Flow Zone Indicator and was estimated to be equivalent to:

$$FZI = \left[\frac{RQI}{\varphi_z}\right]$$

Where, RQI is referred to as the Reservoir Quality Index and φ_z is the pore volume to grain volume ratio. These terms are defined as:

$$RQI = 0.0314 \sqrt{Permeability/Porosity}$$

$$\varphi_z = \left[\frac{\varphi_e}{1 - \varphi_e}\right]$$

Fazelalavi et al (2013) suggest that the FZI method is not always accurate for wells without cores as log based attributes for estimating the necessary terms are not reliable. They proposed establishing a linear relationship between FZI and $(1/S_{wir}\varphi_e)$ based on core data which could then be utilized for uncored wells with similar lithofacies. That is,

$$FZI = \frac{a}{S_{wir}\phi_e} + b$$

Where, S_{wir}, is the reducible water saturation which can be estimated using the NMR log along with ϕ_e. The FZI value for each core sample is calculated from core laboratory data for

permeability and porosity estimate from the MRI log as described above. The constants, *a* and *b*, are to be derived from the best fit correlations.

Pore structure in the Arbuckle however is very complex and there are a lot of variations in pore size distribution (unimodal, bimodal and trimodal) versus depth in very short intervals. Due to this complexity and non-homogeneity in pore size distribution, the Arbuckle permeability at the Wellington site was calculated based on pore size classification (Micro, Meso and Mega pores). FZI in each pore size class was correlated to 1/(Swir*Phi) of the same class. As documented in Table 2, all FZI values less than 2 and 1/(swir*phi) values less than 48 were assigned for micro pore sizes which correspond to permeability values less 0.5 milliDarcy (mD). Similarly, FZI from 2 to 11 and 1/(swir*phi) value from 48 to 106 were considered for meso pore sizes which correspond to permeability from about 0.5 to 25 mD. Finally, FZI from 11-150 and 1/(swir*phi) from 106 to 851 were considered for mega pore sizes which correspond to permeability greater than 25 mD. The ranges are listed in the table below and the correlations are shown in figures 6-8.

Table 2 Ranges of FZI and 1/(Swir*Phi)

Pore Size	**Approximate Permeability (mD)**	**FZI**	**1/(Swir*Phi)**
Micro	<0.5	<2	<48
Meso	0.5-25	2-11	48-106
Mega	>25	11-150	106-851

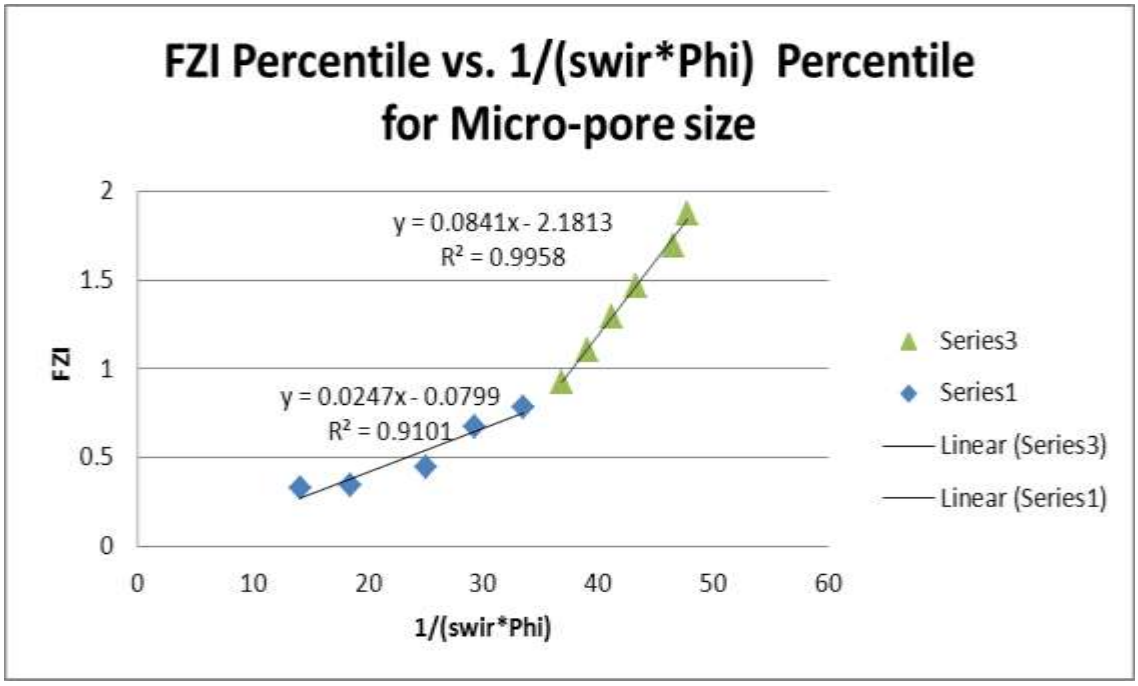

Figure 6 Plot of FZI vs 1/(swir*phi) for micro-pore sizes

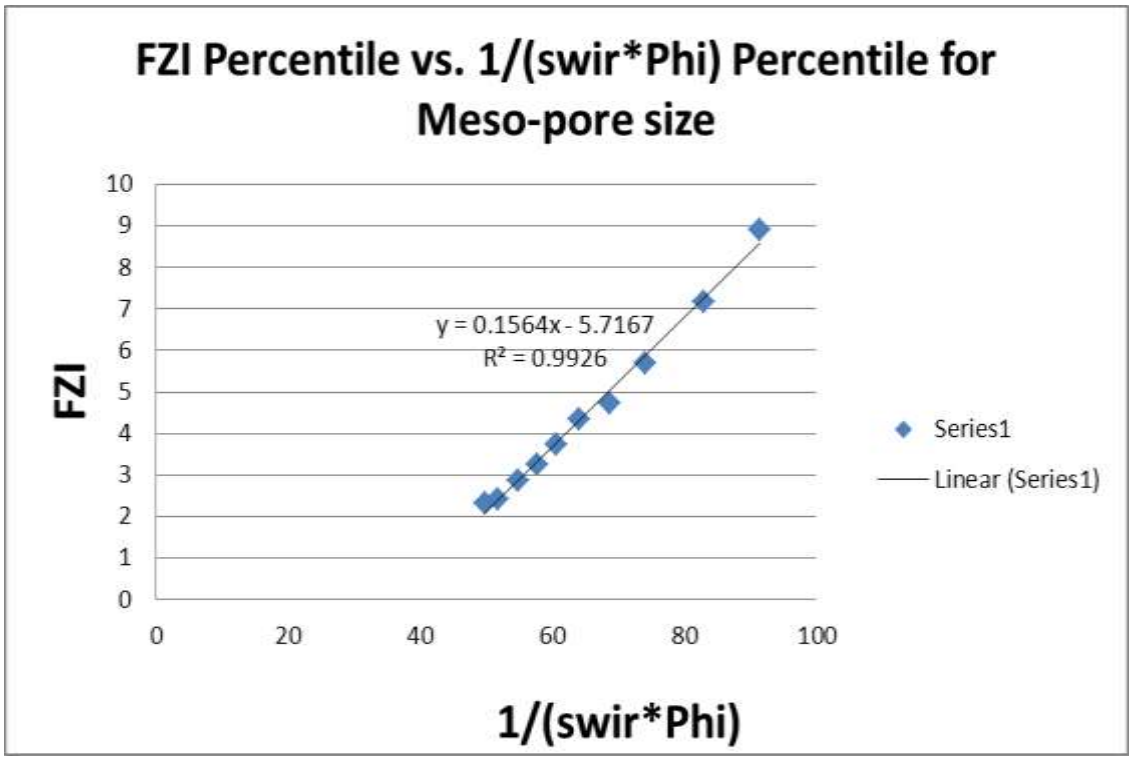

Figure 7 Plot of FZI vs 1/(swir*phi) for meso-pore sizes

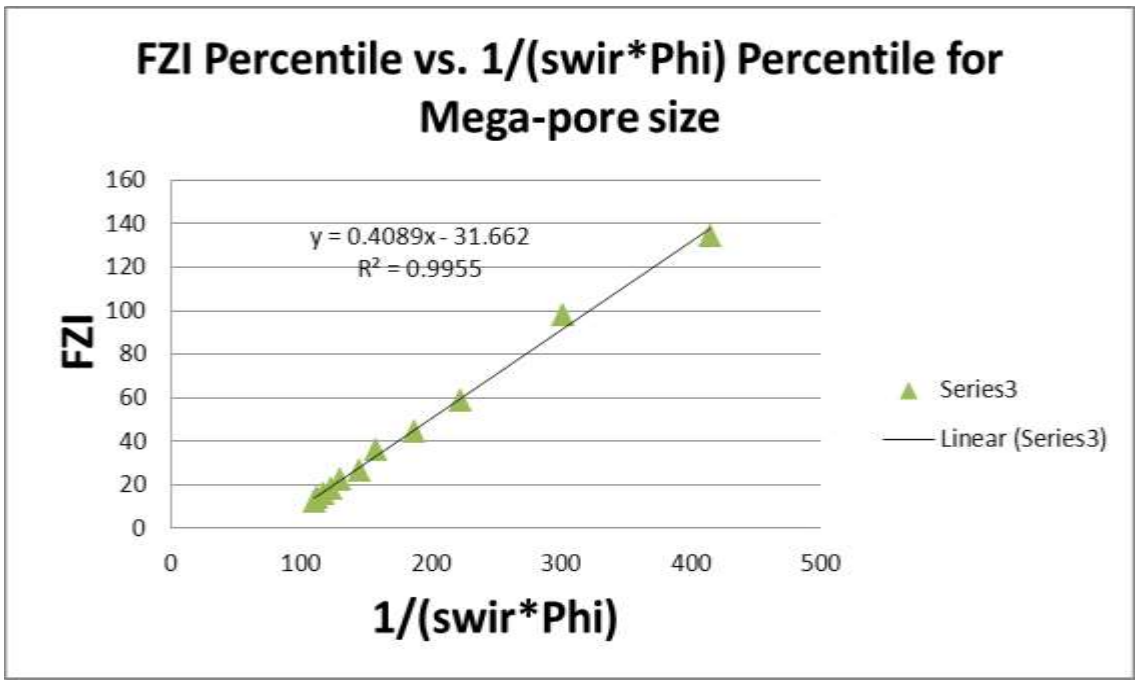

Figure 8 Plot of FZI vs 1/(swir*phi) for mega-pore sizes

The coefficients, *a* and *b,* derived from the correlations in the figures above are documented in the table 3:

Table 3 Correlation coefficients, a and

Pore Size	***a***	***b***	**R2**	**1/(Swir*Phi)**
Micro	0.0247	-0.0779	0.9101	<36
Micro	0.0841	-2.1813	0.996	<48
Meso	0.1564	-5.7167	0.9926	48-106
Mega	0.4089	-31.662	0.9955	>106

The permeability estimated by the FZI-1/(Swir*Phi) method along with the laboratory derived values of this parameter is plotted in Figure 9, from which a fairly good match can be inferred.

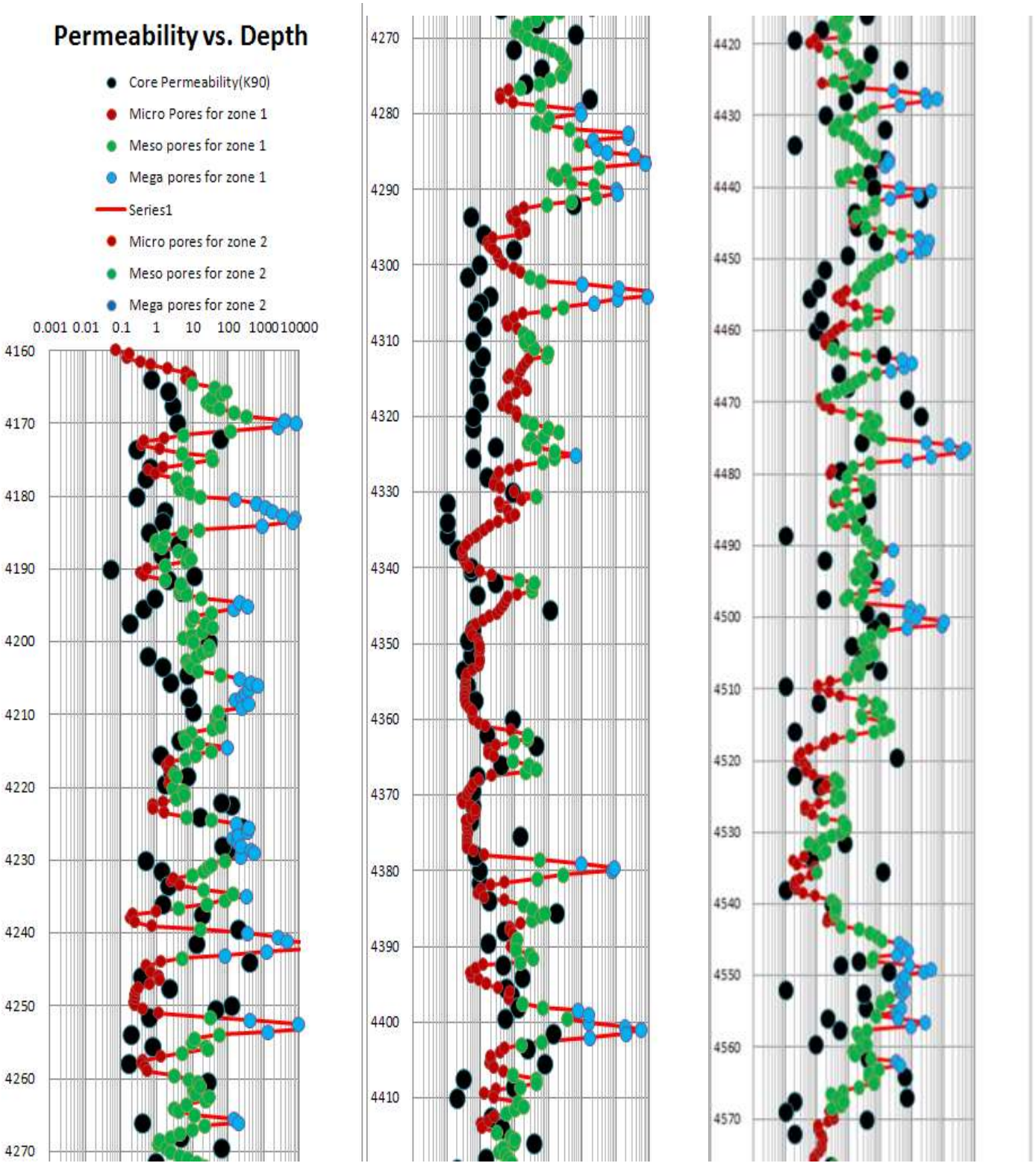
Permeability vs. Depth
Core Permeability(K90)
Micro Pores for zone 1
Meso pores for zone 1
Mega pores for zone 1
Series1
Micro pores for zone 2
Meso pores for zone 2
Mega pores for zone 2
0.001 0.01 0.1 1 10 100 1000 10000
4160
4170
4180
4190
4200
4210
4220
4230
4240
4250
4260
4270
4270
4280
4290
4300
4310
4320
4330
4340
4350
4360
4370
4380
4390
4400
4410
4420
4430
4440
4450
4460
4470
4480
4490
4500
4510
4520
4530
4540
4550
4560
4570

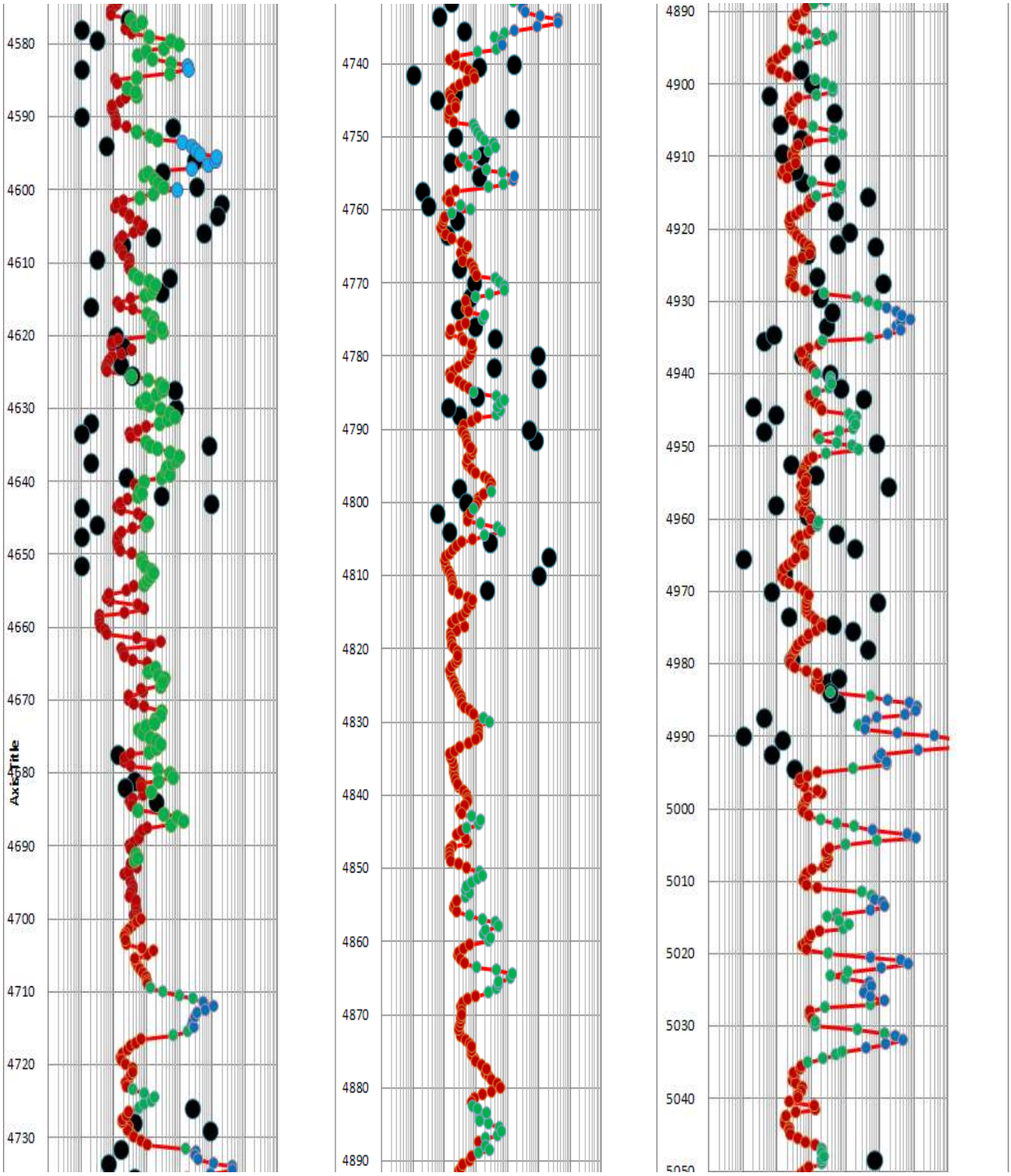
4580
4590
4600
4610
4620
4630
4640
4650
4660
4670
4680
4690
4700
4710
4720
4730
Axis Title
4740
4750
4760
4770
4780
4790
4800
4810
4820
4830
4840
4850
4860
4870
4880
4890
4890
4900
4910
4920
4930
4940
4950
4960
4970
4980
4990
5000
5010
5020
5030
5040
5050

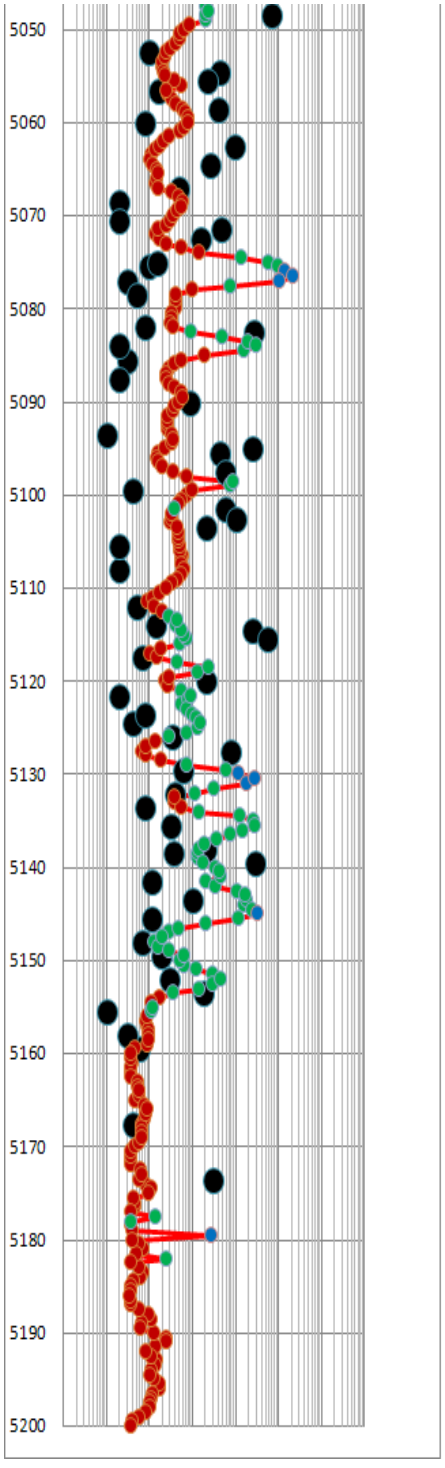

Figure 9 Comparison of laboratory derived and FZI-1/(Swir*Phi) based estimates of hydraulic permeability.

3.3 Permeability of Confining Zone

The National Energy Technology Laboratory (NETL) in Pittsburgh estimated the permeability in the Pierson formation using the Pulse Decay Method (Dicker and Smits, 1988). As shown in Figure 10, results indicated an extremely low permeability of 2.9 and 1.6 nanoDarcy (nD; 10^{-09} Darcy) (Scheffer, 2012).

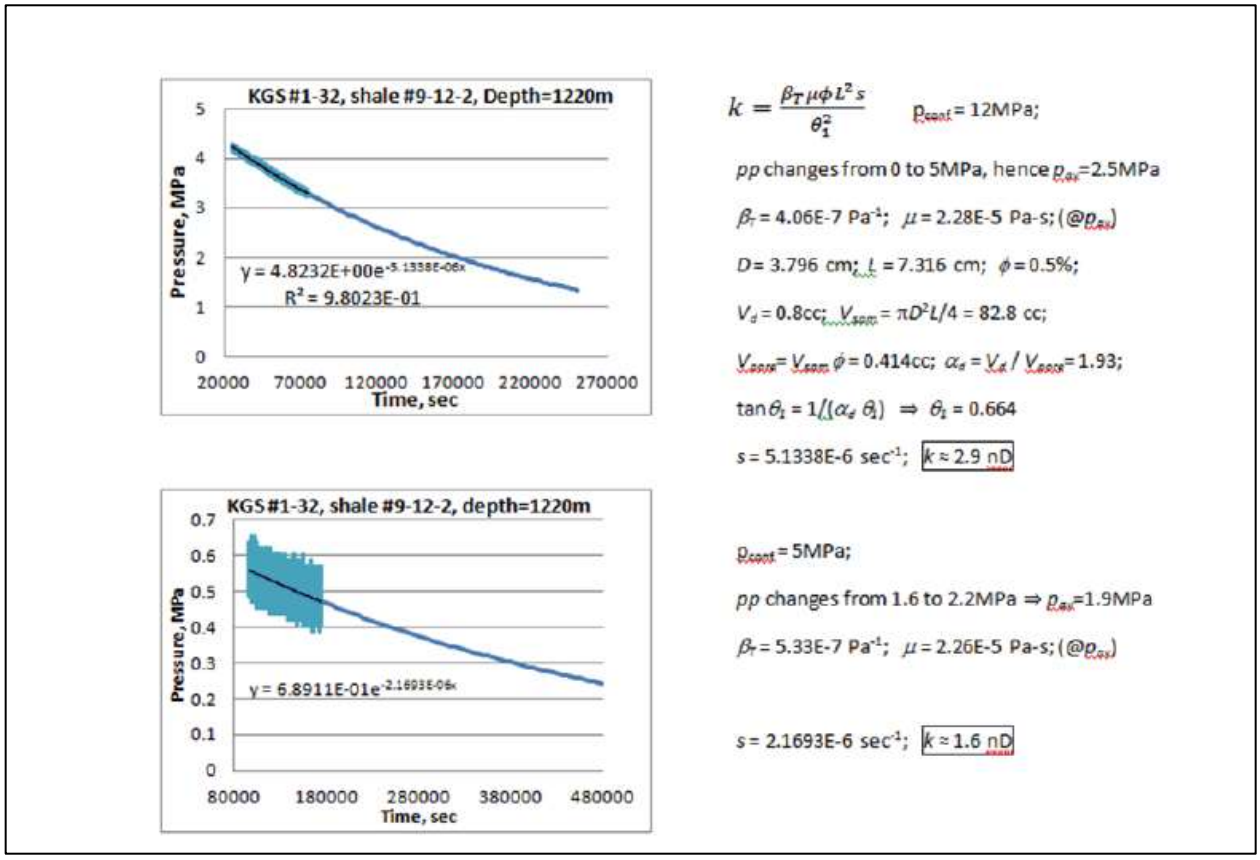

Figure 10 Estimated permeability in the Pierson confining zone.

3.4 Entry Pressure

Entry pressure in the Chattanooga shale was calculated in well 1-32 and 1-28 using the Techlog wellbore software platform by Schlumberger. Techlog first converts pore size (T2 distribution) to estimate the pore throat radius (as a function capillary pressure) using a proportionally constant Kappa (K) according to the following relationship proposed by Volokin and others (2001):

$$K = \frac{P_c}{T_2^{-1}} = \frac{\sigma \cos\theta R_{pore}}{\rho r_{neck}}$$

Where,

K=Kappa

ρ=NMR surface relaxivity

σ = Interfacial tension

θ = Contact angle

r_{neck}= pore throat radius

R_{pore} = pore body radius

Based on calibration at the Spivey-Grab field (Watney et al., 2001) and the Wellington West field (Bhattacharya et al., 2003), a Kappa value of 9 and 15 was used in the confining zone. Capillary pressure and pore throat radius relationship is expressed by the following relationship for mercury-air phase:

$$P_c = \frac{2\sigma cos\theta}{r_{neck}}$$

Where,

P_c = Capillary pressure,

σ = Interfacial tension of Mercury-air,

r_{neck} = pore radius.

The mercury entry pressure for the Simpson shale varies between 7 to 2,260 psi at KGS 1-32 and between 7 to 9,245 psi at KGS 1-28. The following equation was used to convert entry pressure from mercury-air system to CO_2-brine system:

$$Pe_{CO_2/brine} = P_{eHg/air} \frac{\gamma_{CO2/brine}.COS\theta_{CO2/brine}}{\gamma Hg/air.COS\theta_{Hg/air}}$$

where,

$Pe_{CO_2/brine}$ is entry pressure in the $CO_2/brine$ system,

$P_{eHg/air}$ is entry pressure in mercury-air system,

$\gamma_{CO2}/_{brine}$ and $\gamma\, Hg/air$ are interfacial tension of CO_2-brine brine and Hg-air systems respectively,

$COS\theta_{CO2/brine}$and $COS\theta_{Hg/air}$ are contact angles of reservoir CO_2/brine/solid and Hg/air/solid systems.

Interfacial tension of 30 dyne/cm and 485 dyne/cm were used for CO_2-brine and Mercury air systems respectively (Chalbaud et al. 2006). Also, contact angle of 0^o and 140^o were used for CO_2-brine and Mercury-air systems.

Using the above relationship, the maximum entry pressure of approximately 2260 psi (at KGS 1-32) for the mercury-air system is equivalent to 182 psi in the CO_2-brine system. Similarly, the maximum value of approximately 9,245 psi for the mercury-air system at KGS 1-28 is equivalent to 746 psi in the CO_2-brine system. Entry pressure is higher at KGS 1-28 due to the presence of smaller pores at this site as compared to KGS 1-32.

The Chattanooga Shale is expected to provide much more confinement than the Simpson Group underneath it. The maximum entry pressure in the Chattanooga Shale at KGS 1-28 is 11,840 psi in the mercury-air system and 956 psi in the CO_2-brine system. As discussed in the modeling section (Section 5), the maximum induced CO_2 pressure at the top of the Arbuckle/base of the Simpson Shale is approximately 13 psi. Therefore, the primary confining zone is expected to confine the injected CO_2 in the Arbuckle aquifer.

3.5 Three-Dimensional Seismic Survey and Analyses

Various seismic analyses techniques were implemented at the Wellington site to characterize the subsurface formations. The results demonstrate the ability of the seismic techniques to map the key formation horizons, identify faults, estimate formation thickness, and characterize the geologic fabric in the subsurface. Importantly, seismic results verified the lateral continuity of the injection and confining zones, a key demonstration that is necessary to satisfy Class VI permitting requirements. The results also verified the presence of the low permeability baffle zone within the injection interval, which has implications for containing CO_2 within the Arbuckle itself.

3.5.1 Stratigraphic Mapping

Seismic results were analyzed for structural characterization as well as stratigraphic analyses. A zero-phase correlation with appropriately adjusted synthetic seismogram is presented in Figure 11. The presence of a continuous injection zone (Arbuckle Group) and the overlying confining zone (Simpson Group, Chattanooga Shale, and Pierson Formation) can be readily inferred from the figure.

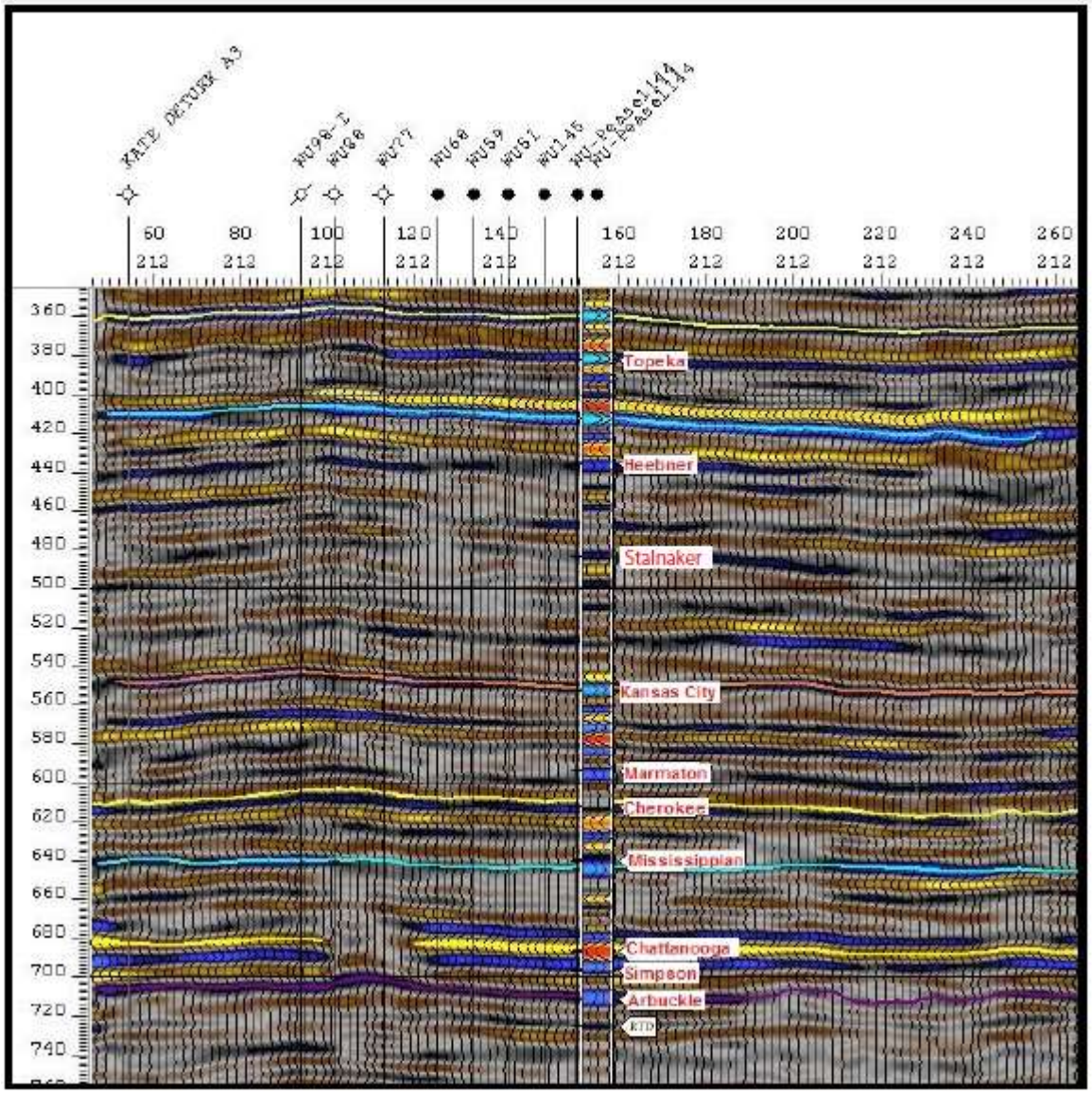

Figure 11 Correlated Arbitrary Profile (color scale = seismic amplitude), illustrating the tie to the synthetic seismogram. The vertical extents of the profile cover a range from approximately 1750 – 4250 feet below surface. Contents of the image are variable density amplitude with conventional wiggle trace overlay. (Y-axis = two-way travel time, in milliseconds; X-axis = distance). Figure 12 presents the index map.

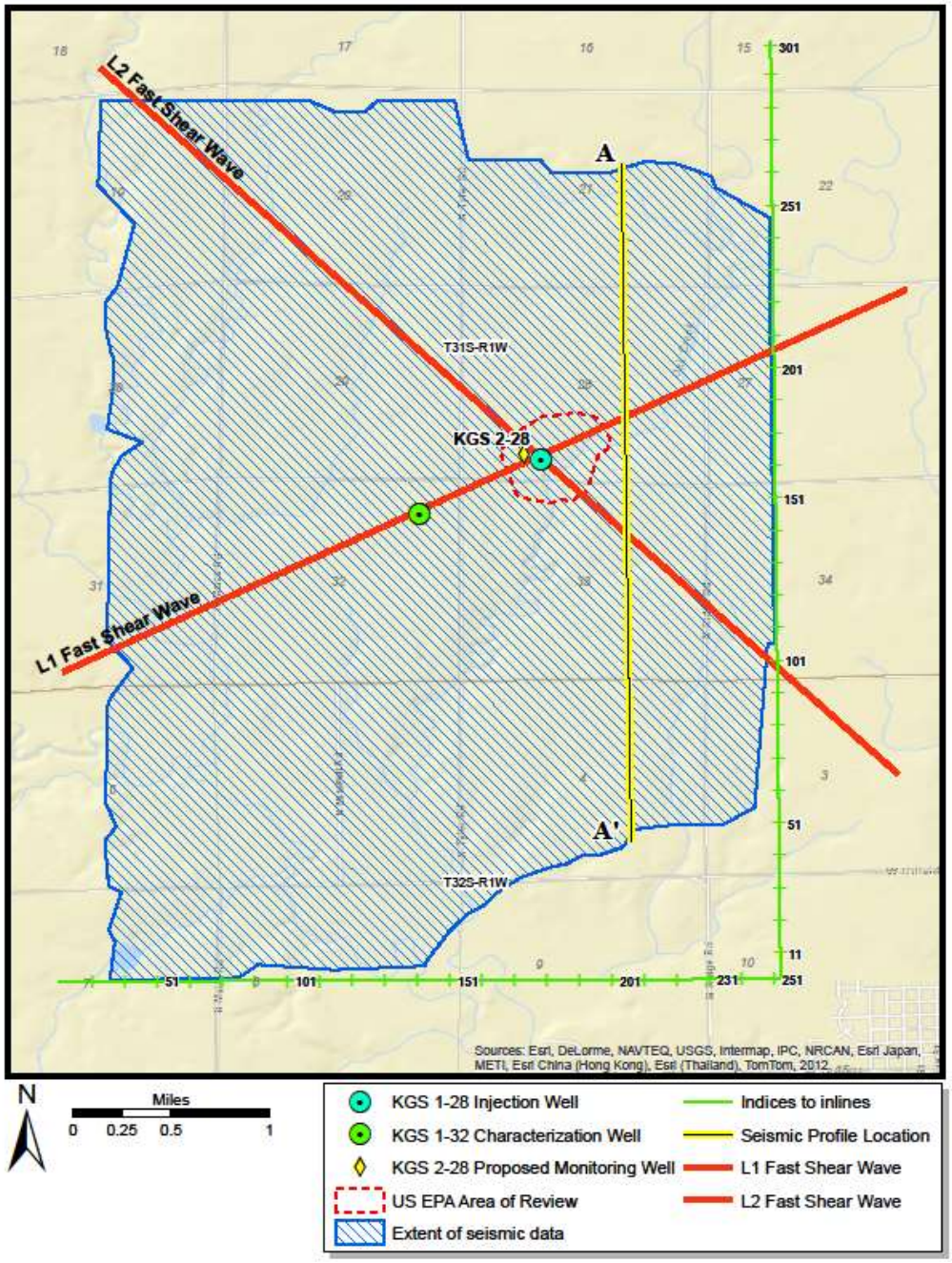

Figure 12 Index Map illustrating the location of the seismic profile shown in Figure 11 (heavy yellow north-south line). Also shown are locations of 2D shear wave profiles, L1 oriented west-southwest-east-northeast and L2 oriented northwest-southeast. Indices to inlines appear on the east edge of the green boundary and indexes to crosslines (also referred to as traces) appear on the south boundary of the green outline. Extents of seismic data are indicated within the red line.

3.5.2 Structure Mapping using Seismic Data

Seismic event tracking within a seismic volume can be rendered in map form, also known as Time Structure mapping. Time structure mapping of the confining zone was performed to confirm the continuity of the continuity of the confining zone at the Wellington site. Figure 13 a-b shows the structure of the top of the confining zone (top of Pierson Formation) and the base of the confining zone (base of Simpson Group/top of Arbuckle group).

Based on the time structure maps of the top and bottom of the confining zone, the thickness of the confining zone was constructed and presented in Figure 14x. In the Wellington area, the thickness varies from approximately 150 ft in the northwest to 250 ft. At the injection well site (KGS 1-28), the seismic based thickness of 230 ft is remarkably close to the geophysical log based thickness of approximately 250 feet estimated from the logs.

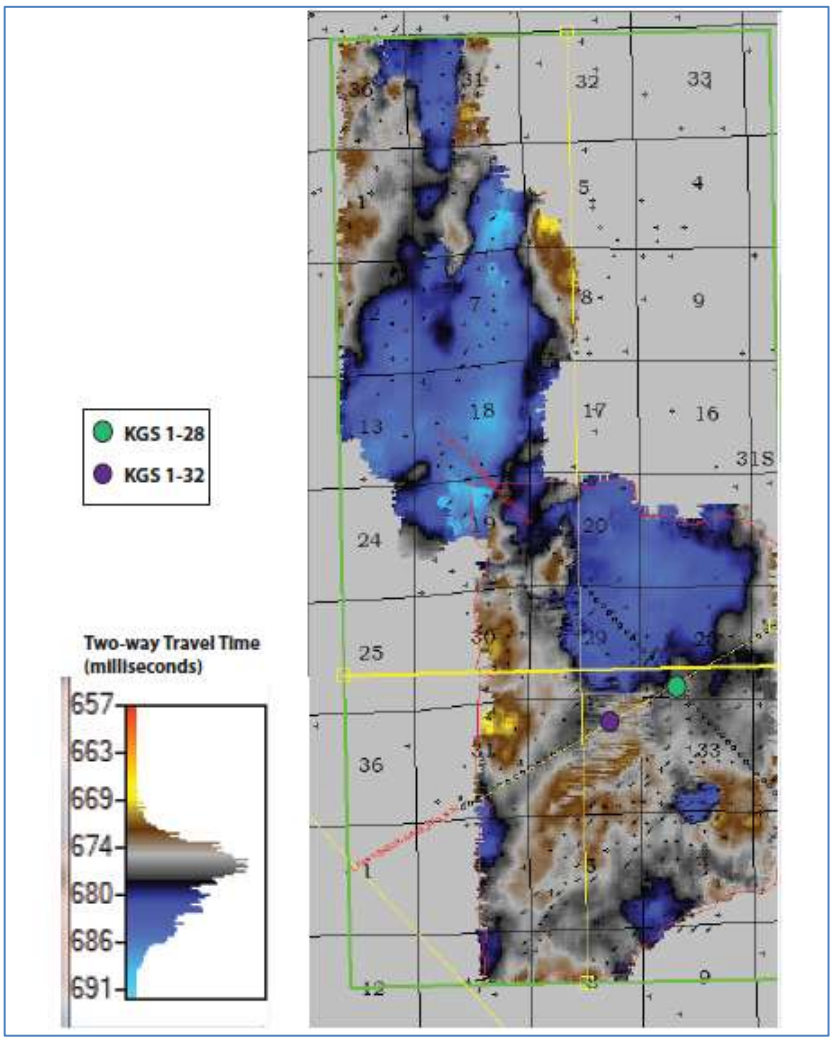

Figure 13-a Time structural variation of the Pierson surface in the Wellington area.

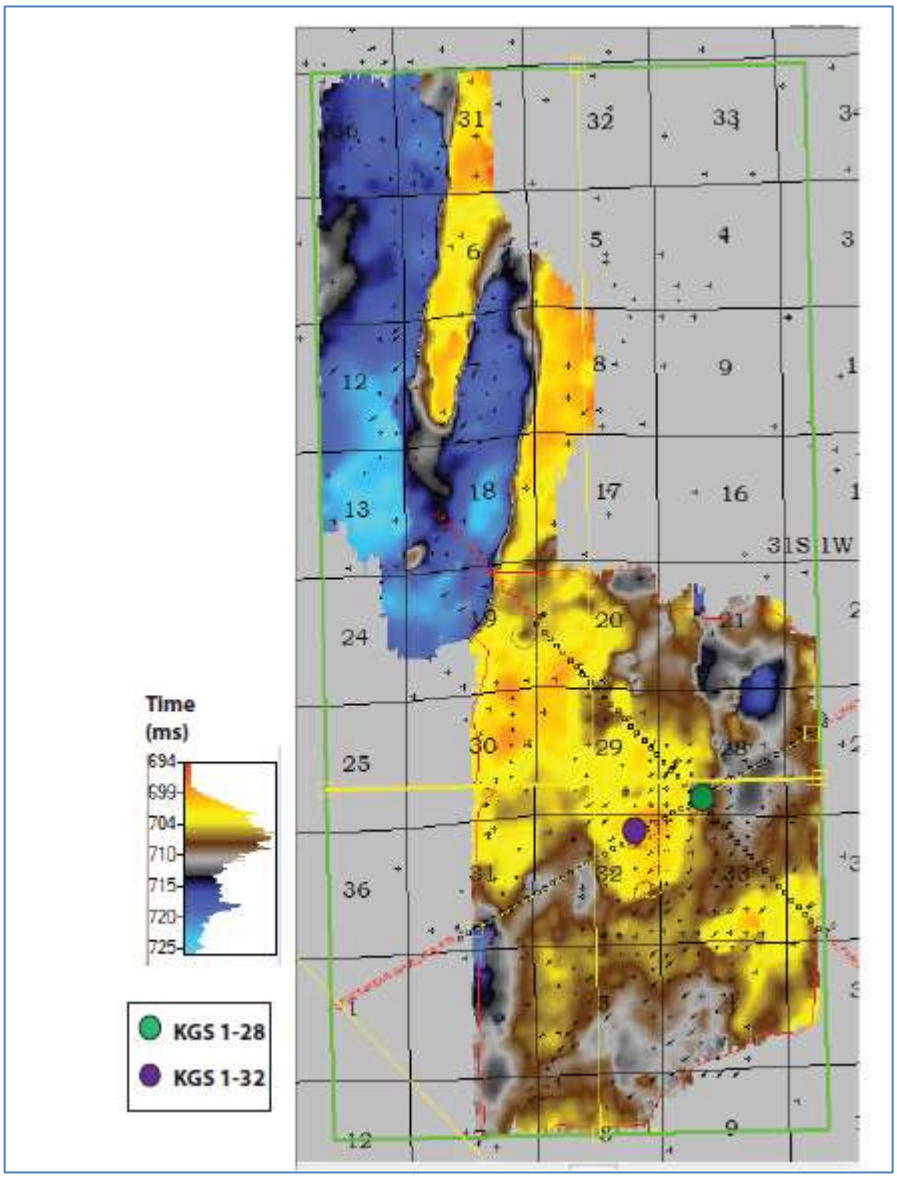

Figure 13-b Time structural variation of the Arbuckle surface (base of Simpson Group).

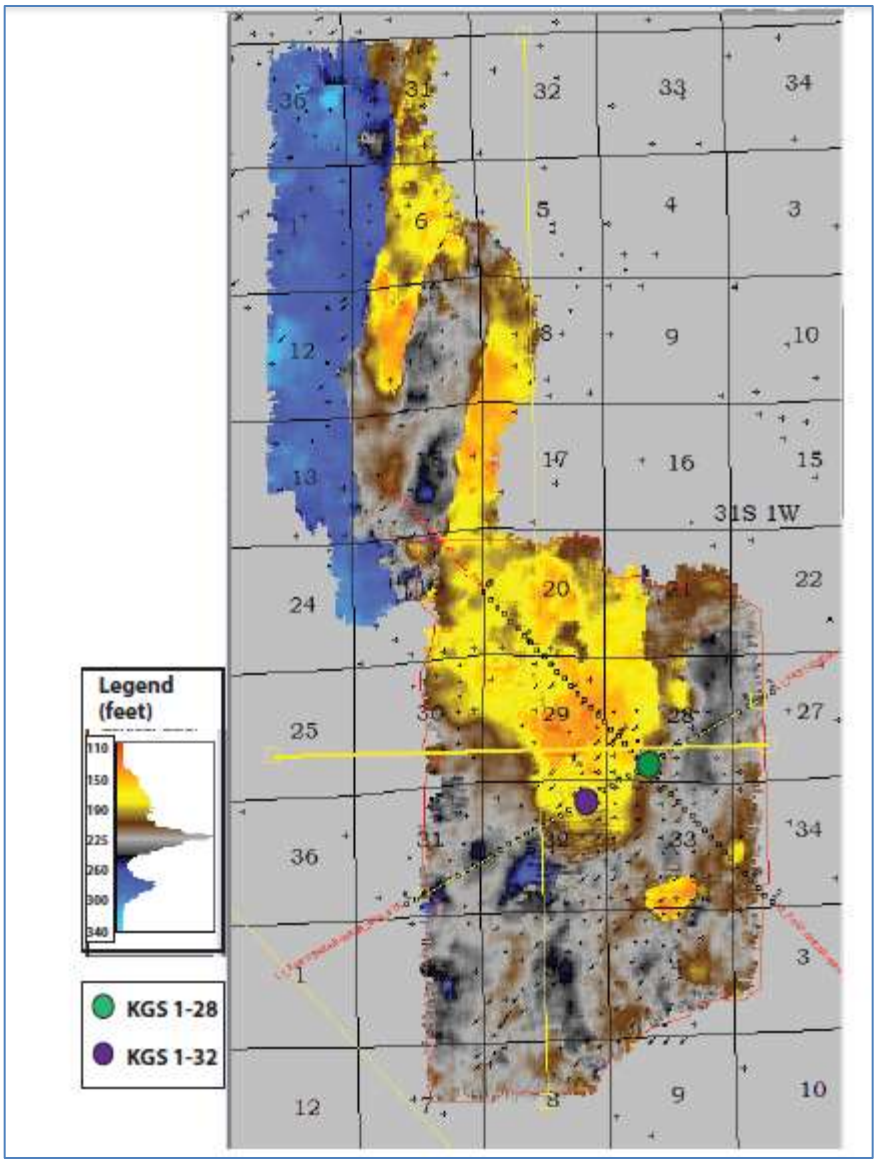

Figure 14 Seismic impedance based thickness (feet) from top of Pierson Formation to top of Arbuckle Group.

3.5.3 Impedance Mapping

A typical profile from the inverted acoustic impedance volume along the north-south seismic profile line shown in Figure 12 is presented in Figure 15. Higher porosity, lower velocity/lower density rocks are indicated in yellow. There is a consistently higher impedance zone in the lower Mississippian at around 680 ms. This unit is overlain by a widespread low impedance (brown and gray color corresponding to the argillaceous siltstone described earlier as the (highly confining)

Pierson Formation. Note also the high impedance strata throughout the Arbuckle which agrees with core, log, and geochemical data which indicates there to be a low permeability baffle zones throughout the Arbuckle. The highest impedance (lowest porosity) zone in the Arbuckle is in the upper third of the Arbuckle which coincides with the thickest low vertical permeability interval from 4290 - 4490ft as shown in Figure 9.

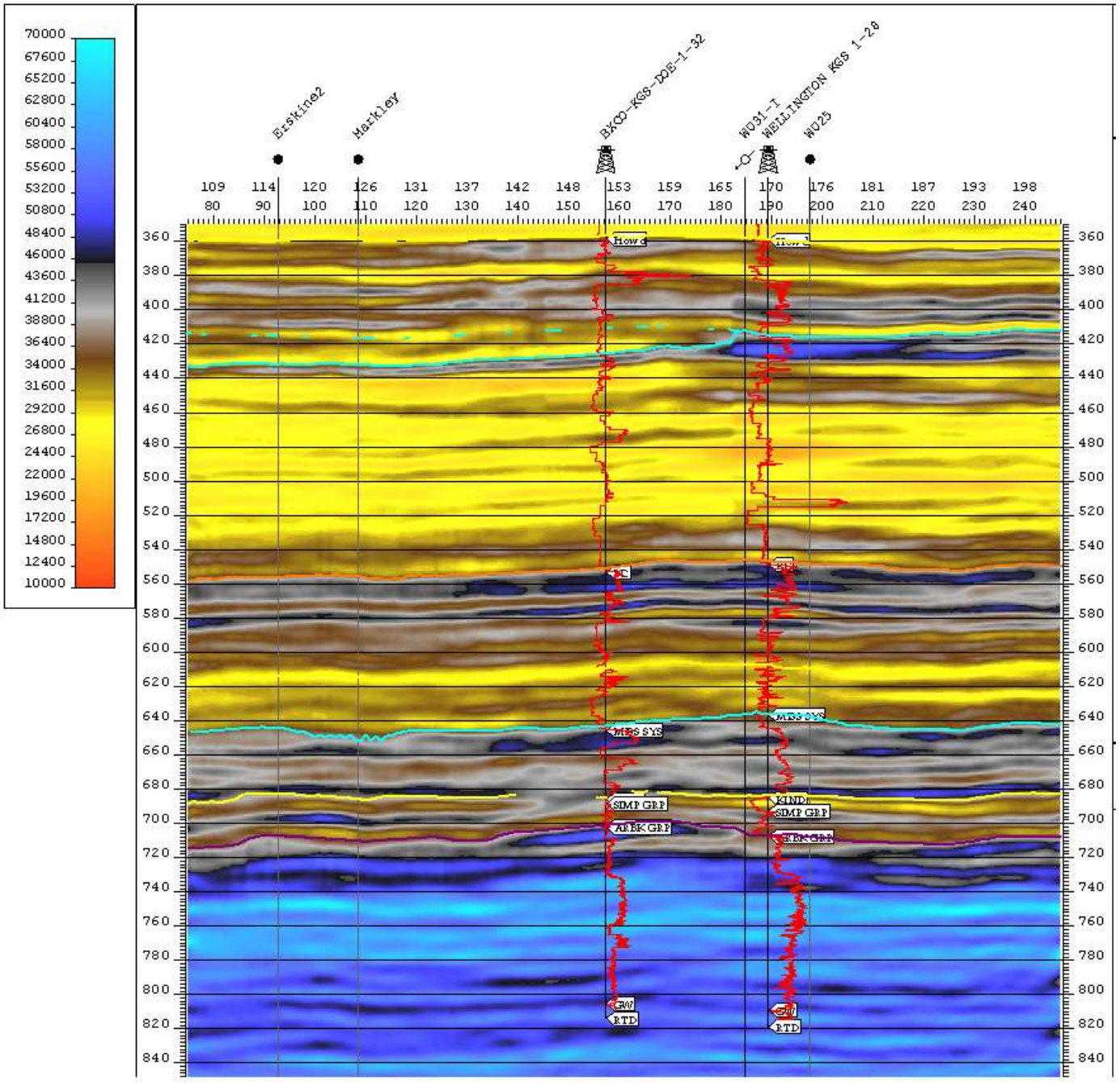

Figure 15 Arbitrary Profile from Acoustic Impedance volume. Log trace overlay (red) from p-wave velocity. Vertical scale two-way travel time, ms. Color scale = acoustic impedance. Profile location shown in Figure 12.

The distribution of average impedance in the Pierson Formation is presented in Figure 16. This map confirms that the Pierson is present throughout the Wellington area with an impedance in the range 37,000-40,000 (ft/sec x g/cm^3). The average impedance in the entire confining zone (base of Simpson Group to top of Pierson Formation) is presented in Figure 17. In general, the average

impedance is slightly lower in the entire confining zone due to the presence of the relatively high porosity Chattanooga Shale. While the Pierson does not have as much shale content as the Chattanooga, the argillaceous siltstone of this formation has extremely low permeability (Nano-Darcy level) as documented above.

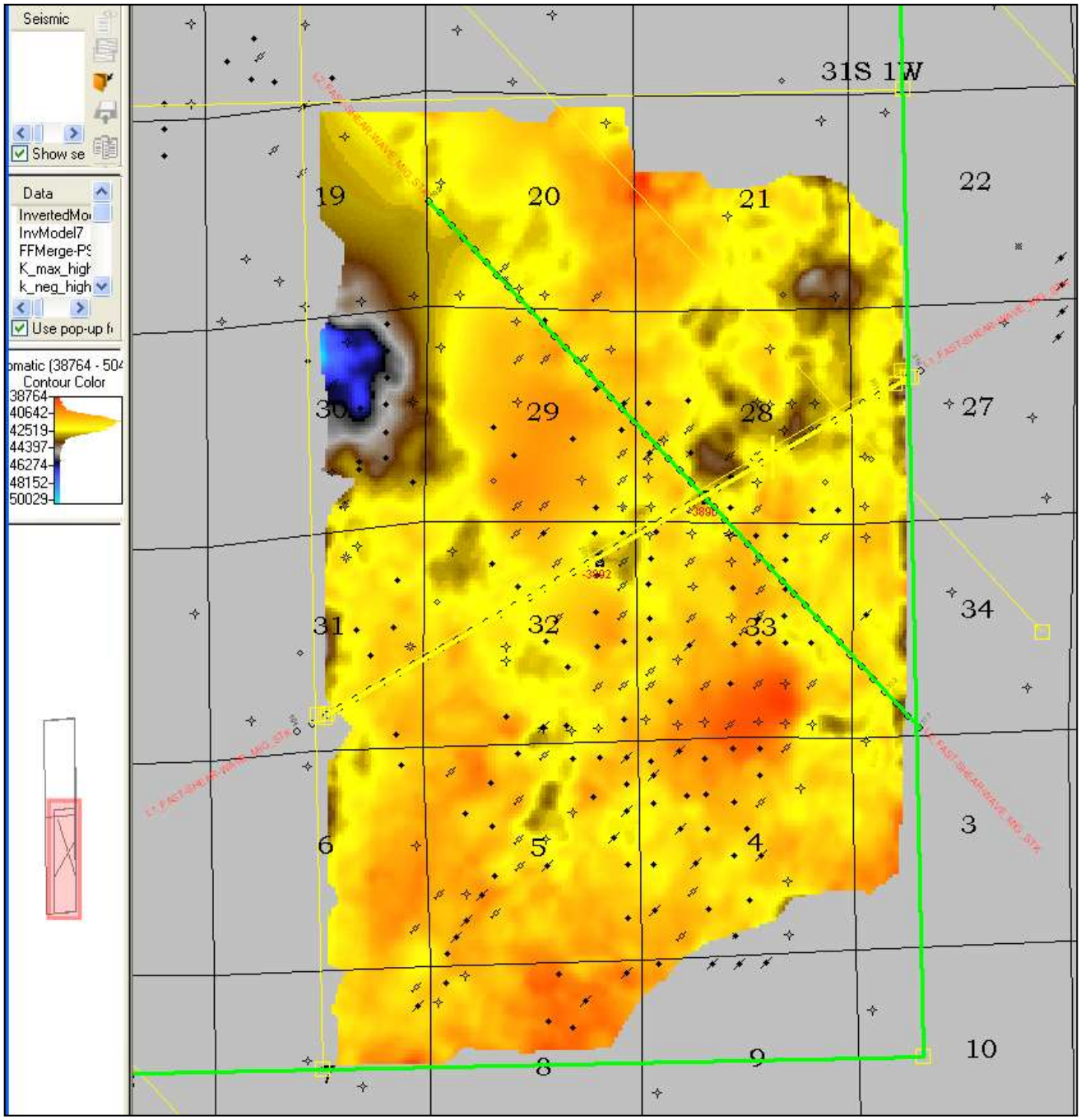

Figure 16 Acoustic Impedance variance within the Lower Mississippian Pierson, the tight argillaceous siltstone.

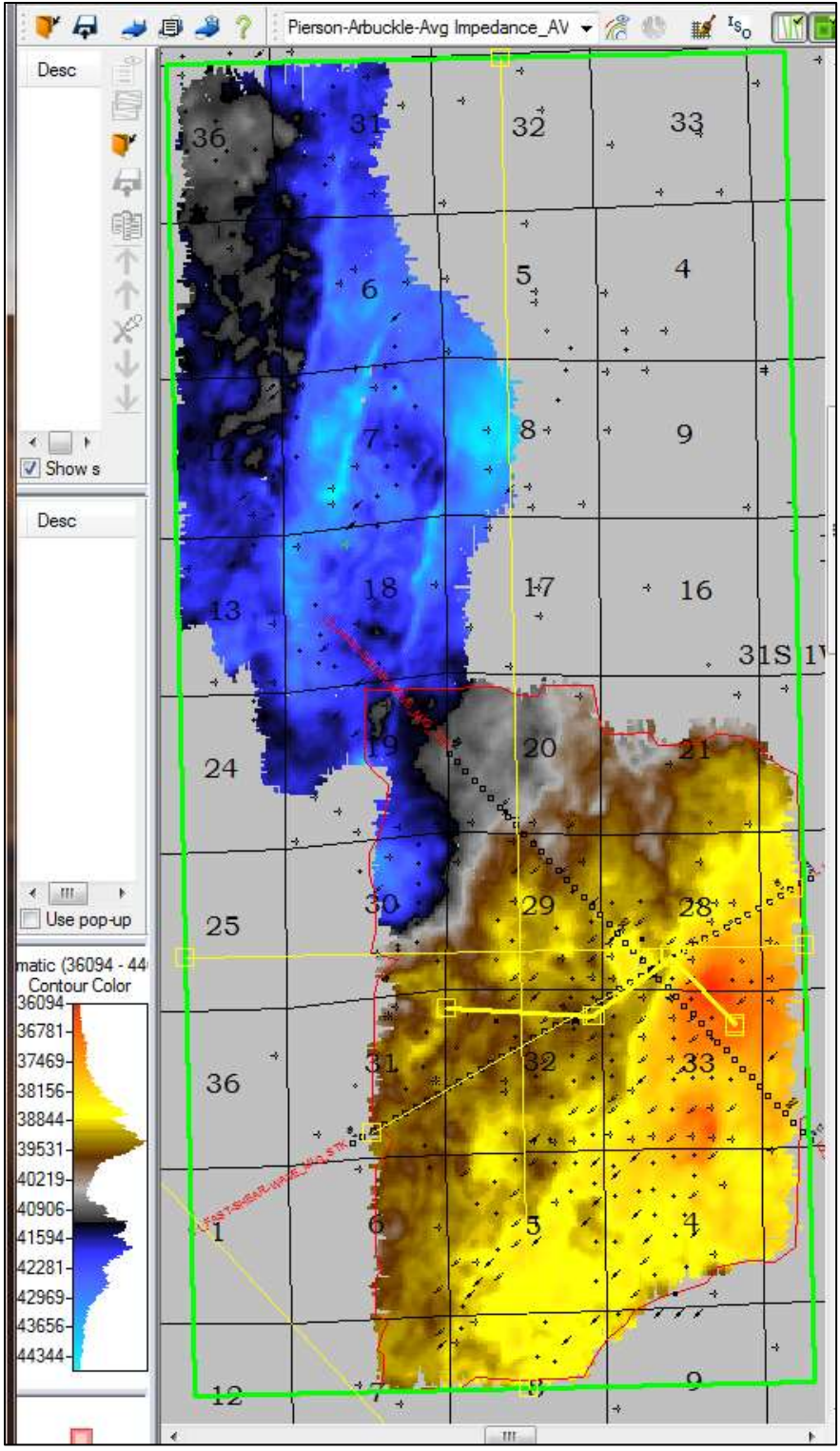

Figure 17 Acoustic impedance variance within the upper confining zone (base of Simpson Group to top of Pierson).

4.0 Validation of Hydrogeologic Characterization

4.1 Geochemical Evidence of a Competent Upper Confining Zone

4.1.1 Ion Composition

Due to their conservative nature, bromine and chlorine are especially useful in differentiating salinity sources and establishing the basis of brine mixture in the subsurface (Whittemore, 2007). Bromine, chlorine, and sulfate concentrations of brine from nine depths in the Arbuckle and three depths in the Mississippian formations were evaluated. The Br^-/Cl^- and SO_4^{2-}/Cl^- weight ratios versus chloride concentration for the Arbuckle saline aquifer and Mississippian reservoir at Wellington are presented in Figure 18 from which it is clear that the geochemical composition of the Mississippian waters is markedly different than that of the Arbuckle. The salinity within the Mississippian varies between approximately 120,000 mg/l and 135,000 mg/l versus approximately 30,500 mg/l in the underlying upper Arbuckle. Similarly, the SO_4^{2-}/Cl^- ratio of approximately 0.002 in the Mississippian formation is significantly different than the range of this ratio of 0.002-0.0055 in the upper Arbuckle. Collectively, the chloride and SO_4^{2-}/Cl^- data suggest a hydraulic separation between the Mississippian and the Arbuckle systems, which supports the conceptualization of a tight upper confining zone.

4.1.2 Isotopic Characterization

Oxygen and hydrogen isotope distributions present another opportunity to assess hydraulic connectivity between the Arbuckle Group and the Mississippian System. Figure 19 shows the δD vs $\delta^{18}O$, reported as the difference between the $^{18}O/^{16}O$ and $^{2}H/^{1}H$ abundance ratios of the samples vs. the Vienna Standard Mean Ocean Water (VSMOW) in per mil notation ($^{o}/_{oo}$) for the Arbuckle and Mississippian samples. Best fit regression lines for each formation, compared with the global meteoric water line (GMWL) and modern seawater is also presented which suggests different water isotopic composition in the Arbuckle and Mississippian systems

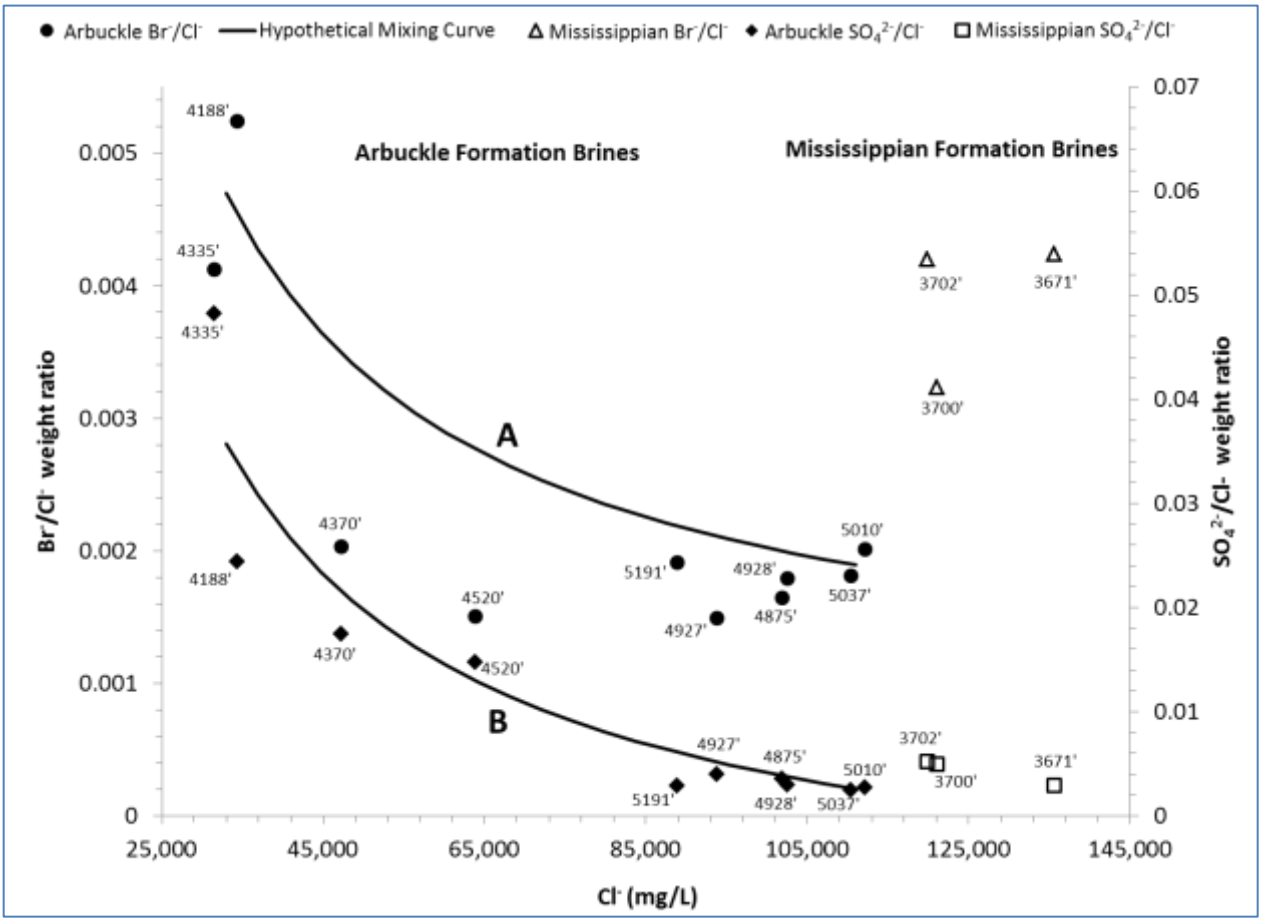

Figure 18 Br^-/Cl^- and SO_4^{2-}/Cl^- weight ratios versus chloride concentration for the Arbuckle saline aquifer and Mississippian oil producing brines at Wellington, Kansas. Also shown are the hypothetical mixing curves for Br^-/Cl^- (A) and SO_4^{2-}/Cl^- (B). Source: Scheffer, 2012.

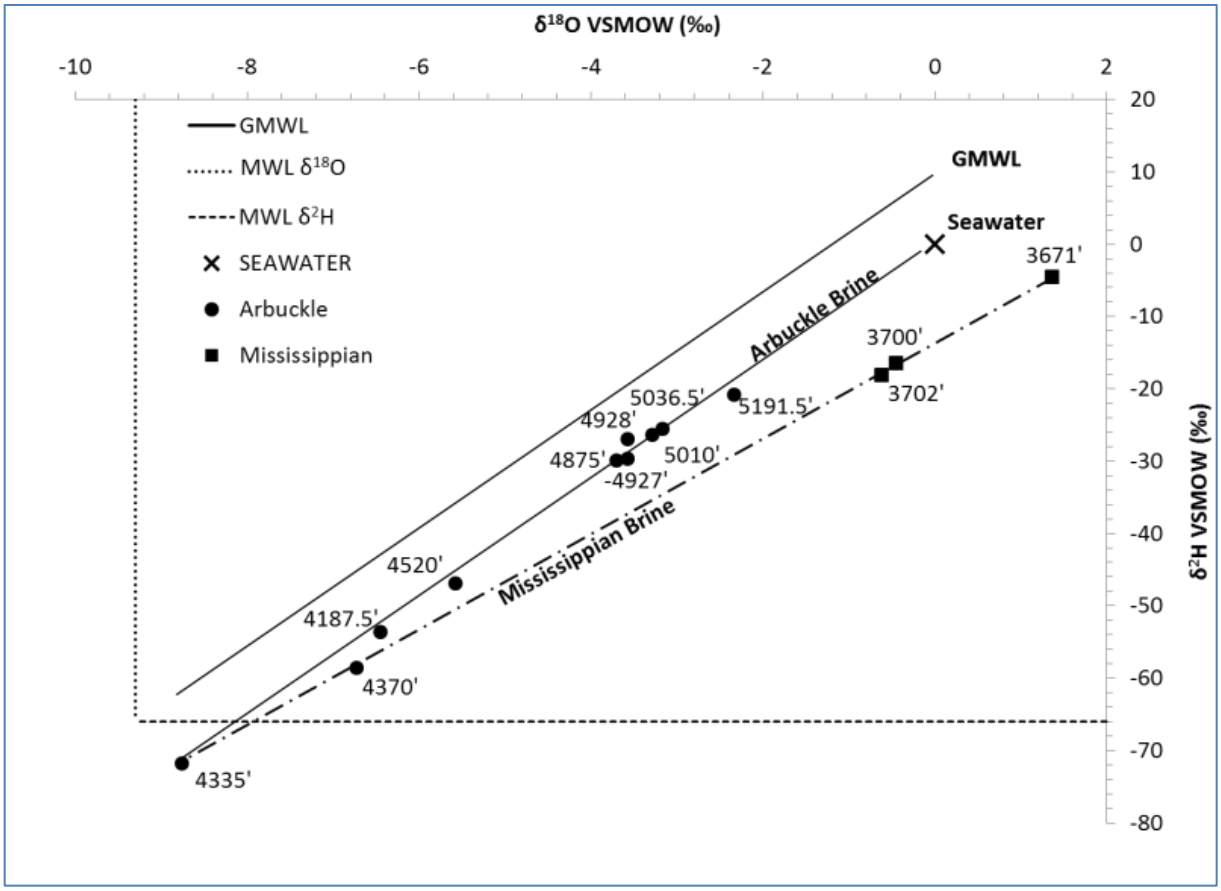

Figure 19 δD vs $\delta^{18}O$ ($^{o}/_{oo}$, VSMOW) for the Arbuckle and Mississippian reservoirs (from Scheffer, 2012).

4.1.3 Chloride Distribution

The chloride distribution in Arbuckle and Mississippian systems at KGS 1-28 and KGS 1-32, obtained from data collected during Drill Stem Testing (DST) and swabbing, is presented in Figure 20. The chloride gradient in the Arbuckle approximates a linear trend with chloride concentration increasing from approximately 30,500 mg/l in the Upper Arbuckle to as much as 118,000 mg/l in the injection zone. Chloride concentration in the Mississippian formation at 119,000 mg/l is substantially higher than in the upper Arbuckle. The large difference in chloride concentrations between the Mississippian and upper Arbuckle supports the conceptualization that the confining zone separating the Arbuckle aquifer from the Mississippian reservoir is tight, and that there are no conductive faults in the vicinity of the Wellington site that hydraulic link the two systems.

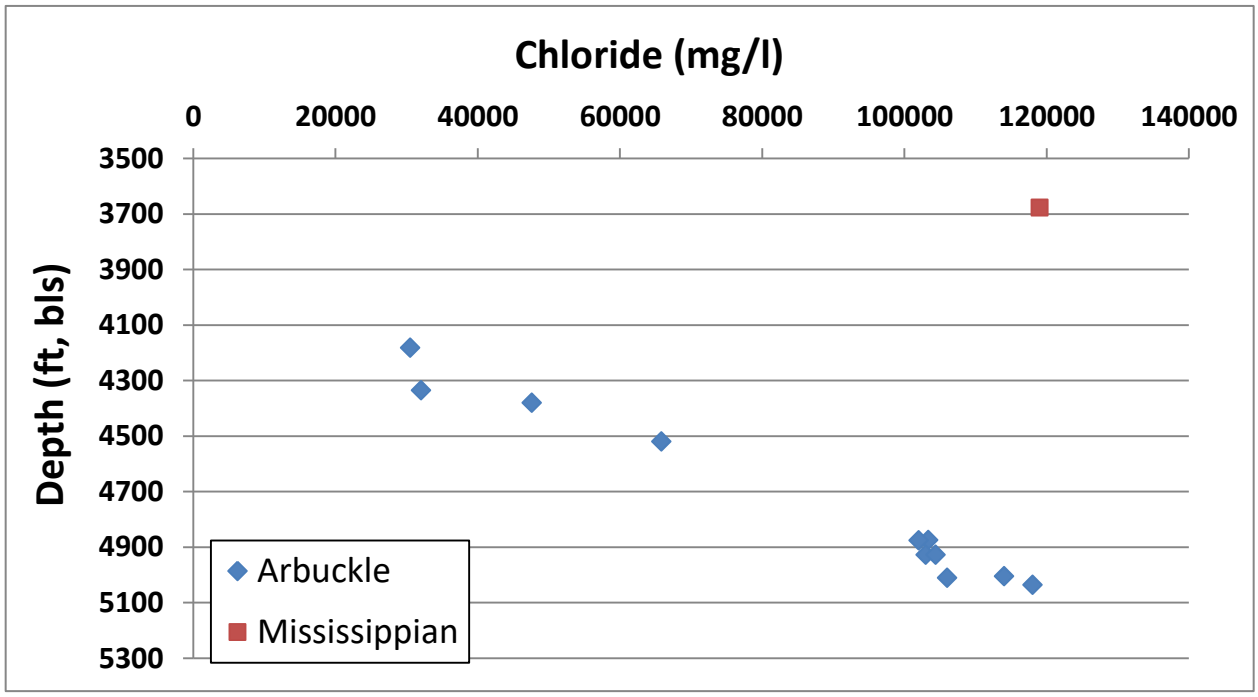

Figure 20 Chloride distribution within the Arbuckle aquifer and Mississippian reservoir at KGS 1-28 and KGS 1-32.

4.2 Pressure Based Evidence of a Competent Confining Zone

The ambient fluid pressure versus depth as measured at KGS 1-32 and KGS 2-18 are plotted in Figure 21. The data presented in this figure indicates that if the Arbuckle pressure gradient (of approximately 0.48 psi/ft) were extended up to a depth of 3664 ft KB in Mississippian, the pressure should be 1506 psi instead of the 1048 psi measured during the DST test. This indicates that the Mississippian is highly under-pressured and is further evidence of a competent confining zone that provides hydraulic impedance between the Arbuckle and Mississippian reservoirs.

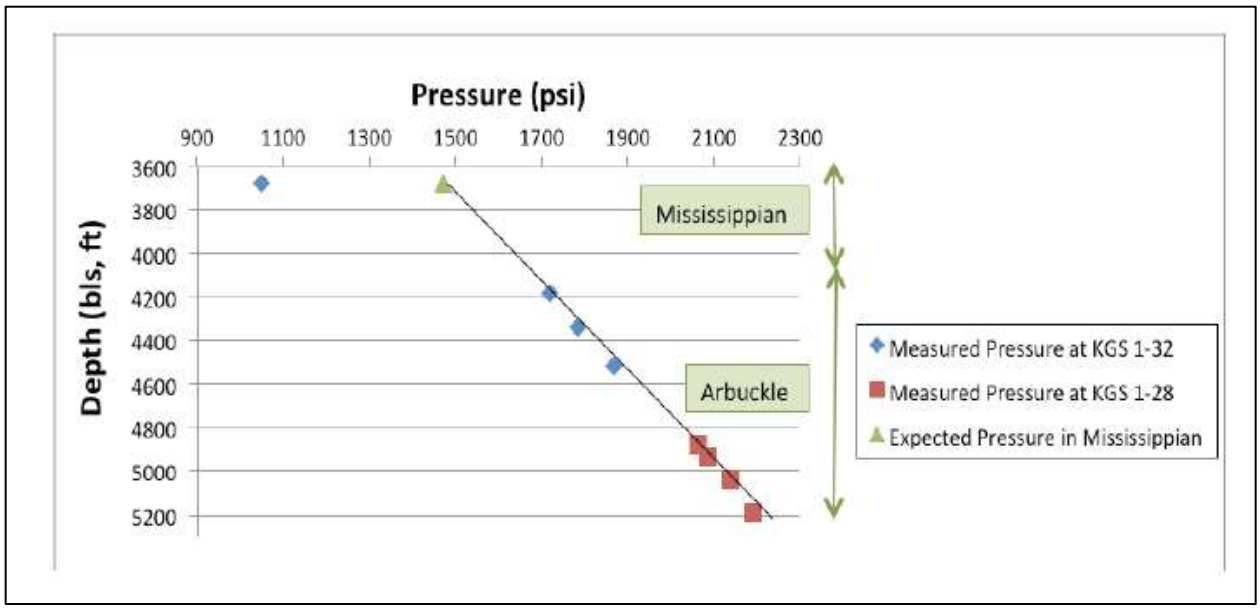

Figure 21 Ambient pressures in the Arbuckle and Mississippian reservoirs as derived from drill stem tests.

4.3 Geochemical Evidence for Stratification of Arbuckle Group

4.3.1 Molar Ratios

Figure 22 shows Ca/Sr molar ratios plotted against Ca/Mg molar ratios of Arbuckle data with trends for dolomitization and calcite recrystallization as described in McIntosh (2004). This plot clearly shows two groupings within the Arbuckle samples. The upper Arbuckle shows a calcite recrystallization signature while the lower Arbuckle shows the influence of dolomitization on brine chemistry. This presents evidence that the upper and lower Arbuckle have different hydrochemical regimes (Barker et al., 2012).

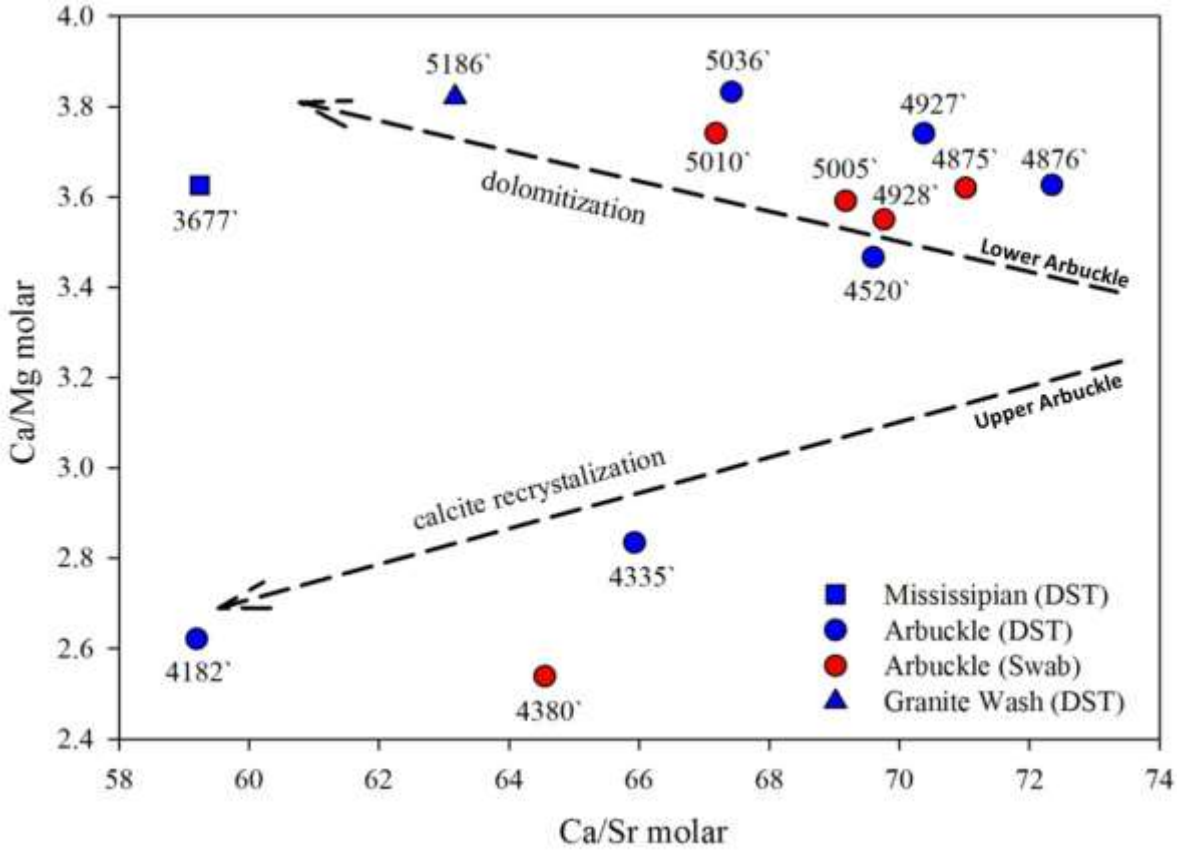

Figure 22 Ca/Sr vs Ca/Mg molar ratios showing trends of dolomitization and calcite recrystallization (from Barker et al., 2012).

4.3.2 Ion Composition

Figure 18 shows Ca/Sr molar ratios plotted against Ca/Mg molar ratios of Arbuckle data with trends for dolomitization and calcite recrystallization as described in McIntosh (2004). This plot clearly shows two groupings within the Arbuckle samples. The upper Arbuckle shows a calcite recrystallization signature while the lower Arbuckle shows the influence of dolomitization on brine chemistry. The data therefore suggests that the upper and lower Arbuckle have different hydrochemical regimes (Barker et al., 2012).

The Br^-/Cl^- ratio provides further evidence of the separation of the upper and lower high permeability zones in the Arbuckle. As can be inferred from Figure 18, the Br^-/Cl^- values of the lower Arbuckle varies over a narrow range in the neighborhood of 0.002, while the variation is much larger (between 0.002 and 0.0055) in the upper Arbuckle. A hypothetical Br-/Cl- mixing

curve (Curve A, Figure 18) was calculated using averaged end-member values from the two deepest samples in the Arbuckle (5010 ft and 5036 ft) and the two shallowest samples in the Arbuckle (4182 ft and 4335 ft) to examine mixing of reservoir fluids for purposes of evaluating connectivity throughout the reservoir. In the lower Arbuckle samples, Br^-/Cl^- concentrations remained relatively consistent, but increased sharply in the upper Arbuckle. This suggests possible different brine origins for the lower and upper regions of the Arbuckle. Regardless of the origin, the data suggests that the brines in the upper and lower Arbuckle are distinctly different and there does not appear to be any mixing between the two zones; supporting the hypothesis of the presence of low permeability baffle zone between the upper Arbuckle and the lower injection interval which was also inferred from the permeability data.

The SO_4^{2-}/Cl^- ratio also supports the suggestion of weak hydraulic connection of the upper and lower intervals of the Arbuckle. The SO_4^{2-}/Cl^- values of the lower Arbuckle show a similar trend as the Br^-/Cl^- in that it spans a very narrow interval in the lower Arbuckle, but varies over a larger range in the upper Arbuckle. A hypothetical SO_4^2/Cl- mixing curve (Curve B, Figure 18) was calculated using end-member values to examine mixing of reservoir fluids and evaluate connectivity throughout the reservoir. As with the bromine data, a substantially different ratio and a poor fit in the upper Arbuckle provides additional support to the hypothesis that the upper and lower Arbuckle zones are not in hydraulic communication (Scheffer, 2012).

4.3.3 Isotopic Characterization

Oxygen and hydrogen isotope distributions also point to absence of a strong hydraulic connection between the upper and lower parts of the Arbuckle Group. This can be inferred from Figure 19, which shows δD vs $\delta^{18}O$, reported as the difference between the $^{18}O/^{16}O$ and $^2H/^1H$ abundance ratios. The brines from the lower Arbuckle (4875-5036 ft) cluster tightly together and have values distinct from those of the upper Arbuckle (4186-4521 ft). The similarity of the brine from the lower Arbuckle strongly suggests active communication within the lower Arbuckle. In contrast, brines of the upper Arbuckle (4182 and 4335 ft) show more variability suggesting a less vigorous flow system. The upper Arbuckle brines also have distinctly different δD and $\delta^{18}O$

values the lower Arbuckle. This suggests that the lower Arbuckle may not be hydraulically well connected to the upper Arbuckle.

4.3.4 Biogeochemistry

The concentration of the redox reactive ions ferrous iron, sulfate, nitrate, and methane (Fe^{2+}, SO_4^{2-}, NO_3^-, CH_4) can be used as evidence of biological activity in the subsurface (Scheffer, 2012). In oxygen restricted sediments that are rich in organic carbon such as the Arbuckle, stratification would follow the redox ladder with aerobes at shallower depths where oxygen is available, followed by nitrate, iron, and sulfate reducers (in this order), and methanogens at the deepest level based on availability of terminal electron acceptors. Because there is a paucity of oxygen in the Arbuckle, typical stratification of microbial metabolisms would involve dissimilar iron reducing bacteria (DIRB) above sulfate reducing bacteria (SRB) above methanogens. This biogenic stratification would be manifested by a zone with increased reduced iron over decreasing sulfate (or increasing sulfide) over increasing methane. However, as shown in Figure 24 there appears to be two separate trends observed in the Arbuckle aquifer; one trend 4.40, for samples above the suspected baffle (1277 m; 4190 ft to 1321 m; 4334 ft) in the upper Arbuckle, and one trend below the suspected baffle (1378 m; 4521 ft to 1582 m; 5190 ft) in the lower Arbuckle. This suggests a reset of the biogeochemistry due to lack of hydraulic communication between the Upper and Lower Arbuckle.

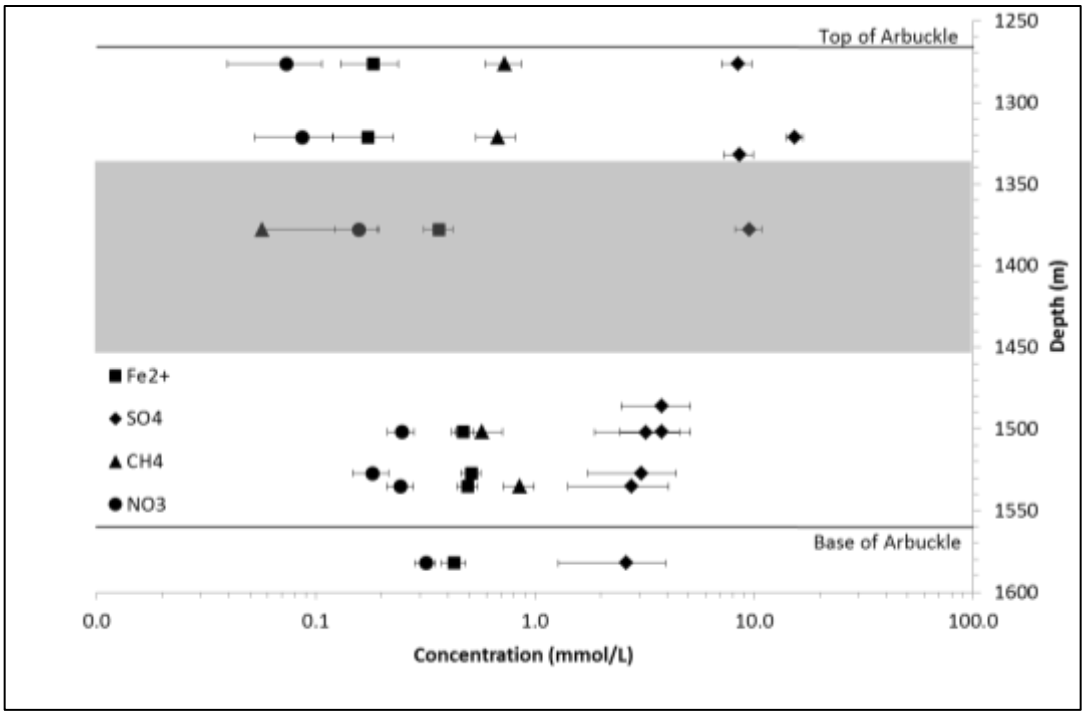

Figure 24 Concentrations of redox reactive ions; ferrous iron, sulfate, methane, and nitrate (Fe^{2+}, SO_4^{2-}, CH_4, NO_3^-) in the Arbuckle reservoir (from Scheffer, 2012).

Microbial Diversity

The biomass concentrations and microbial counts also indicate the presence of a highly stratified Arbuckle reservoir. Biomass concentrations of 2.1 $x10^6$, 1.9 x 10^7 and 2.6 x 10^{-3} cells/ ml were determined using the quantitative polymerase chain reaction (qPCR) procedures at depths of 1277m (4190ft), 1321m (4334ft), and 1378m (4520ft) respectively (Figure 25). The lowest biomass coincides with the low permeability baffle zone in the mid Arbuckle (1378 m; 4520 ft). Decreased flow through the baffle zone could decrease nutrient recharge and lead to nutrient depletion (Scheffer, 2012). The highest biomass and most unique sequences occurred in the upper Arbuckle at 1321 m (4334 ft) as shown in Figure 25.

The free-living microbial community was also examined in the Arbuckle aquifer. Results show 43% diversity at a depth of 1277 m (4190 ft), 62% diversity at 1321 m (4334 ft), and 39% diversity at 1378 m (4520 ft), which follows the same trend as biomass shown in Figure 25B. Notably, the microbial communities from 1277 m (4190 ft) and 1321 m (4334 ft) are very similar to one another and vary distinctly from the community detected at 1378 m (4520 ft). Nine genera of bacteria were detected at 1277 m (4190 ft) and 1321 m (4334 ft). Seven genera of bacteria were detected at 1378 m (4520 ft). *Alkalibacter, Bacillus and Erysipelthrix* were found at the two shallower depths but not at 1378 m (4520 ft). *Dethiobacter* was detected only at the deeper depth of 1378 m (4520 ft).

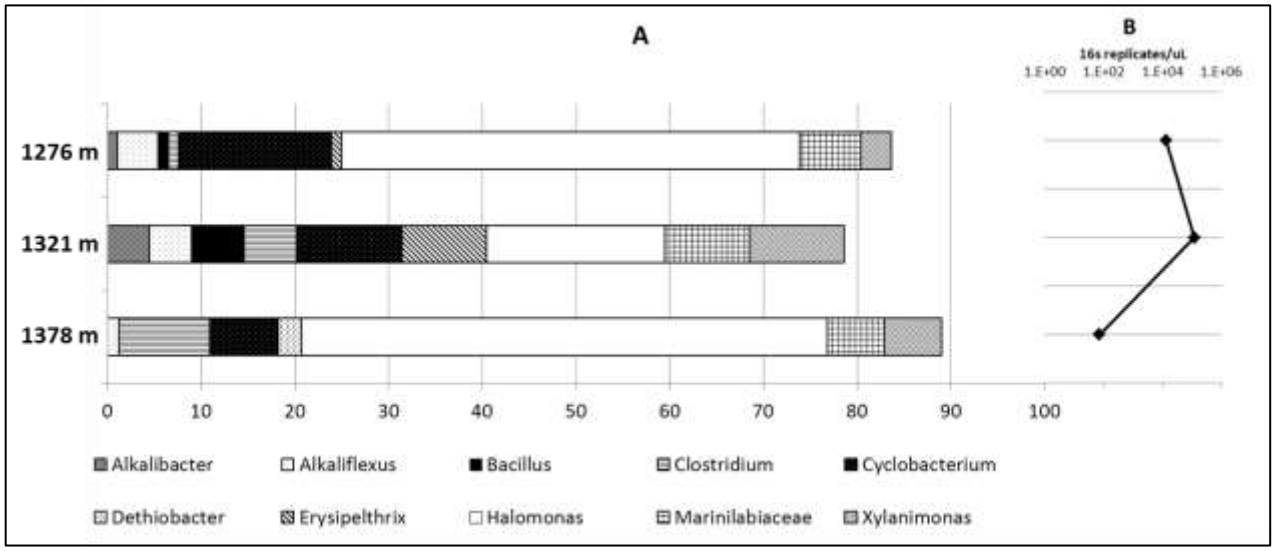

Figure 25 Arbuckle aquifer microbial profile showing the distribution of bacteria in the Arbuckle (A), and the DNA concentration (B) (from Scheffer, 2012).

5.0 Geostatistical Reservoir Characterization of Arbuckle Group

Statistical reservoir geomodeling software packages have been used in the oil and gas industry for decades. The motivation for developing reservoir models was to provide a tool for better reconciliation and use of available hard and soft data (Figure 26). Benefits of such numerical models include: 1) transfer of data between disciplines, 2) a tool to focus attention on critical unknowns, and 3) a 3-D visualization tool to present spatial variations to optimize reservoir development. Other reasons for creating high-resolution geologic models include:

- volumetric estimates
- multiple realizations permit unbiased evaluation of uncertainties prior to finalizing a drilling program
- lateral and top seal analyses
- integration (i.e., by gridding) of 3-D seismic surveys and their derived attributes
- assessments of 3-D connectivity
- flow simulation-based production forecasting using different well designs
- optimizing long-term development strategies to maximize return on investment

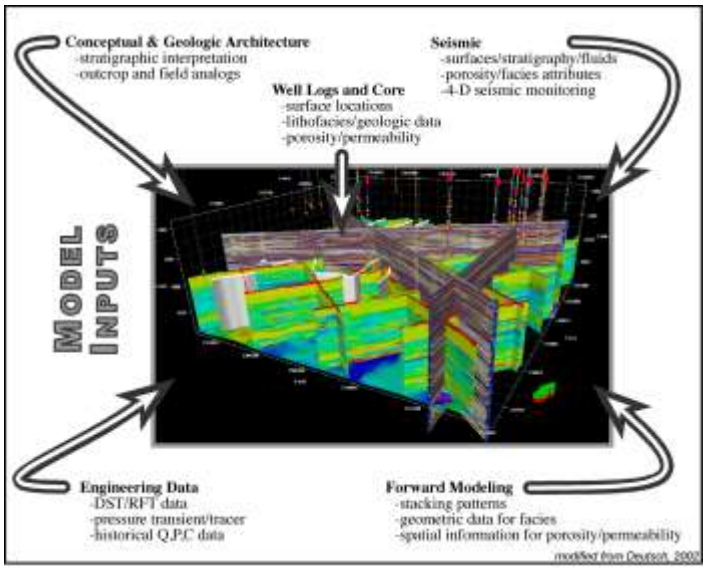

Figure 26 A static, geocellular reservoir model showing the categories of data that can be incorporated (source: modified from Deutsch, 2002).

Although geocellular modeling software has largely flourished in the energy industry, its utility can be important for reservoir characterization in CO_2 research and sequestration projects, such as the Wellington Field. The objective in the Wellington project is to integrate various data sets of different scale into a cohesive model of key petrophysical properties; especially porosity and permeability. The general steps for applying this technology are to model the large-scale features followed by modeling progressively smaller, more uncertain, features. The first step applied at the Wellington field was to establish a conceptual depositional model and its characteristic stratigraphic layering. The stratigraphic architecture provided a first-order constraint on the spatial continuity of facies, porosity, permeability, saturations, and other attributes within each layer. Next, facies (i.e., rock fabrics) were modeled for each stratigraphic layer using cell-based or object-based techniques. Porosity was modeled by facies and conditioned to "soft" trend data such as seismic inversion attribute volumes. Likewise, permeability was modeled by facies and collocated, co-Kriged to the porosity model.

5.1 Conceptual Model

Lower Arbuckle core from Wellington reflect sub-meter-scale, shallowing-upward peritidal cycles. The two common motifs are cycles passing from basal dolo-mudstones/wackestones into algal dolo-laminites or matrix-poor monomict breccias. Bioclasts are conspicuously absent. Breccias are clast-supported, monomictic, angular, and their matrix dominantly consists of cement (Figure 27). They are best classified as crackle to mosaic breccias (Loucks, 1999) because there is little evidence of transportation. Lithofacies and stacking patterns (i.e., sub-meter scale, peritidal cycles) are consistent with an intertidal to supratidal setting. Breccia morphologies, scale (<0.1 m), mineralogy (e.g., dolomite, anhydrite, length-slow chalcedony) depositional setting, greenhouse climate, and paleo-latitude (~15º S) support mechanical breakdown processes associated with evaporite dissolution. The Arbuckle–Simpson contact (~800-ft above the proposed injection interval) records the super-sequence scale, Sauk–Tippecanoe unconformity, which records subaerial-related karst landforms across the Early Phanerozoic supercontinent Laurentia.

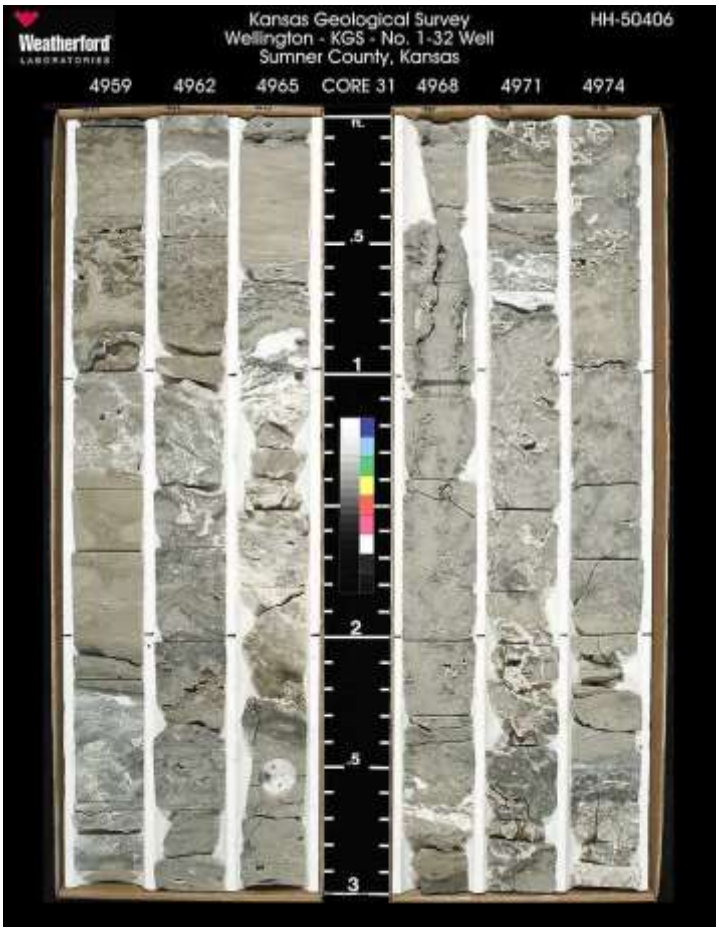

Figure 27 Example of the carbonate facies and porosity in the injection zone in the lower Arbuckle(part of the Gasconade Dolomite Formation). Upper half is light olive gray, medium-grained dolomitic packstone with crackle breccia. Scattered subvertical fractures and limited cross stratification. Lower half of interval shown has occasional large vugs that crosscut the core consisting of a light olive gray dolopackstone that is medium grained. Variable sized vugs range from cm-size irregular to subhorizontal.

5.2 Facies Modeling

The primary depositional lithofacies were documented during core description at KGS 1-32. A key issue was reconciling (order of magnitude) inconsistencies between permeability measurements derived from wireline logs (i.e., nuclear resonance tool), whole core, and step-rate tests. Poor core recovery from the injection zone resulted from persistent jamming, which is commonly experienced in fractured or vuggy rocks. Image logs acquired over this interval record some intervals with large pores (cm-scale) that are likely solution-enlarged vugs (touching-vugs of Lucia, 1999; Figure 28). Touching-vug fabrics commonly form a reservoir-scale, interconnected pore system characterized by Darcy-scale permeability. It is hypothesized that a touching-vug pore

system preferentially developed within fracture-dominated crackle and mosaic breccias—*formed in response to evaporite removal*—which functioned as a strataform conduit for undersaturated meteoric fluids (Figure 29). As such, this high-permeability, interwell-scale, touching-vug pore system is largely strataform and, therefore, predictable.

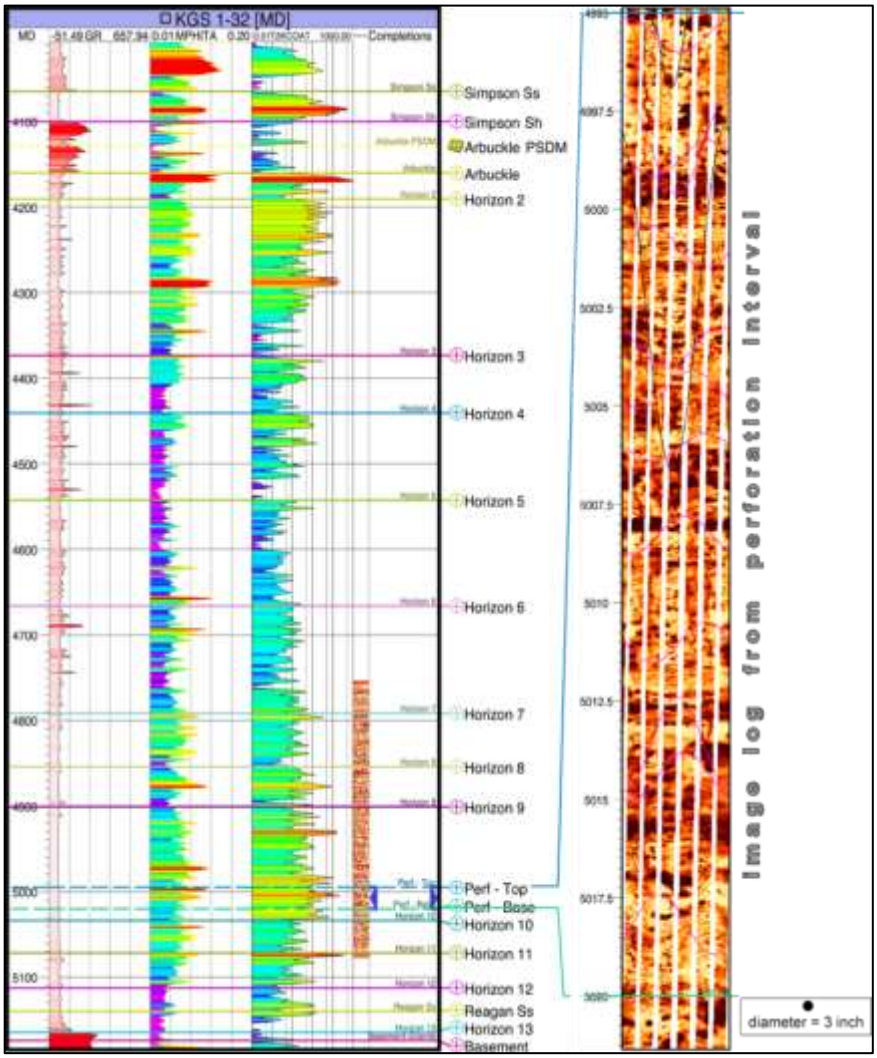

Figure 28 Geophysical logs within Arbuckle Group at KGS 1-32.

(Notes: MPHITA represents Haliburton porosity. Horizon marker represent porosity package. Image log on right presented to provide example of vugs; 3 inch diameter symbol represents size of vug).

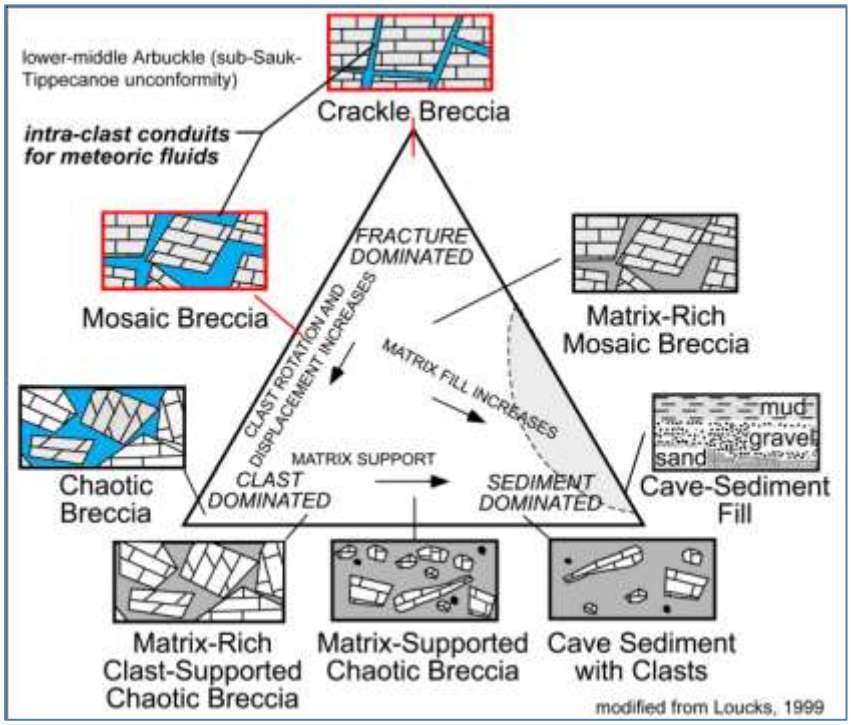

Figure 29 Classification of breccias and clastic deposits in cave systems exhibiting relationship between chaotic breccias, crackle breccias, and cave-sediment fill (source: Loucks, 1999).

5.3 Petrophysical Properties Modeling

The approach taken for modeling a particular reservoir can vary greatly based on available information and often involves a complicated orchestration of well logs, core analysis, seismic surveys, literature, depositional analogs and statistics. Due to the availability of well log data in only two wells (KGS 1-28 and KGS 1-32) penetrating the Arbuckle reservoir at the Wellington site, the geologic model also relied on seismic data, Step Rate Test and Drill Stem Test information. Schlumberger's Petrel™ geologic modeling software package was used to produce a geologic model of the Arbuckle saline aquifer for the pilot project area. This geomodel is 1075 ft deep; spanning the Arbuckle injection interval, the middle baffle zones, and upper Arbuckle high permeability/high porosity zone, as well as a portion of the sealing units (Simpson/Chattanooga shale).

5.3.1 Porosity Modeling

In contrast to well data, seismic data is areally extensive over the reservoir and is, therefore, of great value for constraining facies and porosity trends within the geomodel. Petrel's volume attribute processing (i.e., genetic inversion) was used to derive a porosity attribute from the Pre-Stack Depth Migration (PSDM) volume to generate the porosity model (Figure 30). The seismic volume was created by re-sampling (using the original exact amplitude values) the PSDM 50 feet above the Arbuckle and 500 feet below the Arbuckle (i.e., approximate basement). The cropped PSDM volume and conditioned porosity logs were used as learning inputs during neural network processing. A correlation threshold of 0.85 was selected and 10,000 iterations were run to provide the best correlation. The resulting porosity attribute was then re-sampled, or upscaled (by averaging), into their corresponding 3-D property grid cell.

The porosity model was constructed using Sequential Gaussian Simulation (SGS). The porosity logs were upscaled using arithmetic averaging. The raw upscaled porosity histogram was used during SGS. The final porosity model was then smoothed. The following parameters were used as inputs:

I. Variogram
   a. Type: spherical
   b. Nugget: 0.001
   c. Anisotropy range and orientation
      i. Lateral range (isotropic): 5000 ft
      ii. Vertical range: 10-ft
II. Distribution: actual histogram range (0.06–0.11) from upscaled logs
III. Co-Kriging
   a. Secondary 3-D variable: inverted porosity attribute grid
   b. Correlation coefficient: 0.75

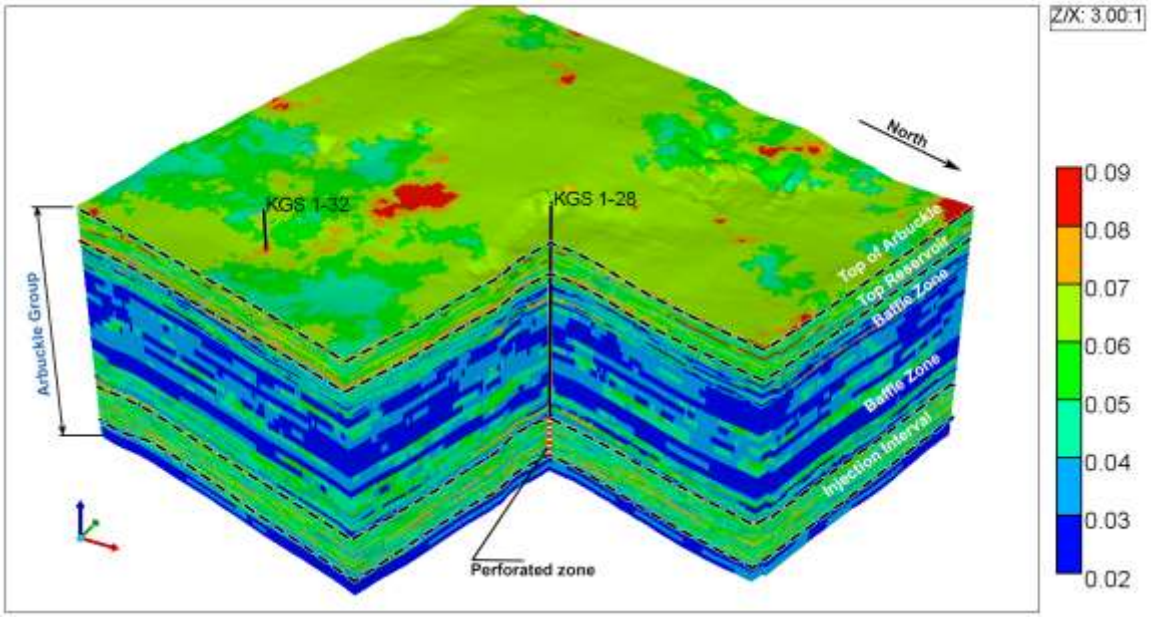

Figure 30 Porosity model of Arbuckle Group derived using the Petrel geostatistical reservoir characterization software.

Permeability Modeling

Upscaled permeability logs were created using the following controls: geometric averaging method; logs were treated as points; and method was set to simple. The permeability model was constructed using Sequential Gaussian Simulation (SGS). Isotropic semi-variogram ranges were set to 3000-ft horizontally and 10-ft vertically. The permeability was collocated and co-Kriged to the porosity model using the calculated correlation coefficient (~0.70). The resulting SGS based horizontal permeability distribution is presented in Figure 31. An east-west cross-section of horizontal permeability through the injection well (KGS 1-28) shows the relatively high permeability zone selected for completion within the injection interval.

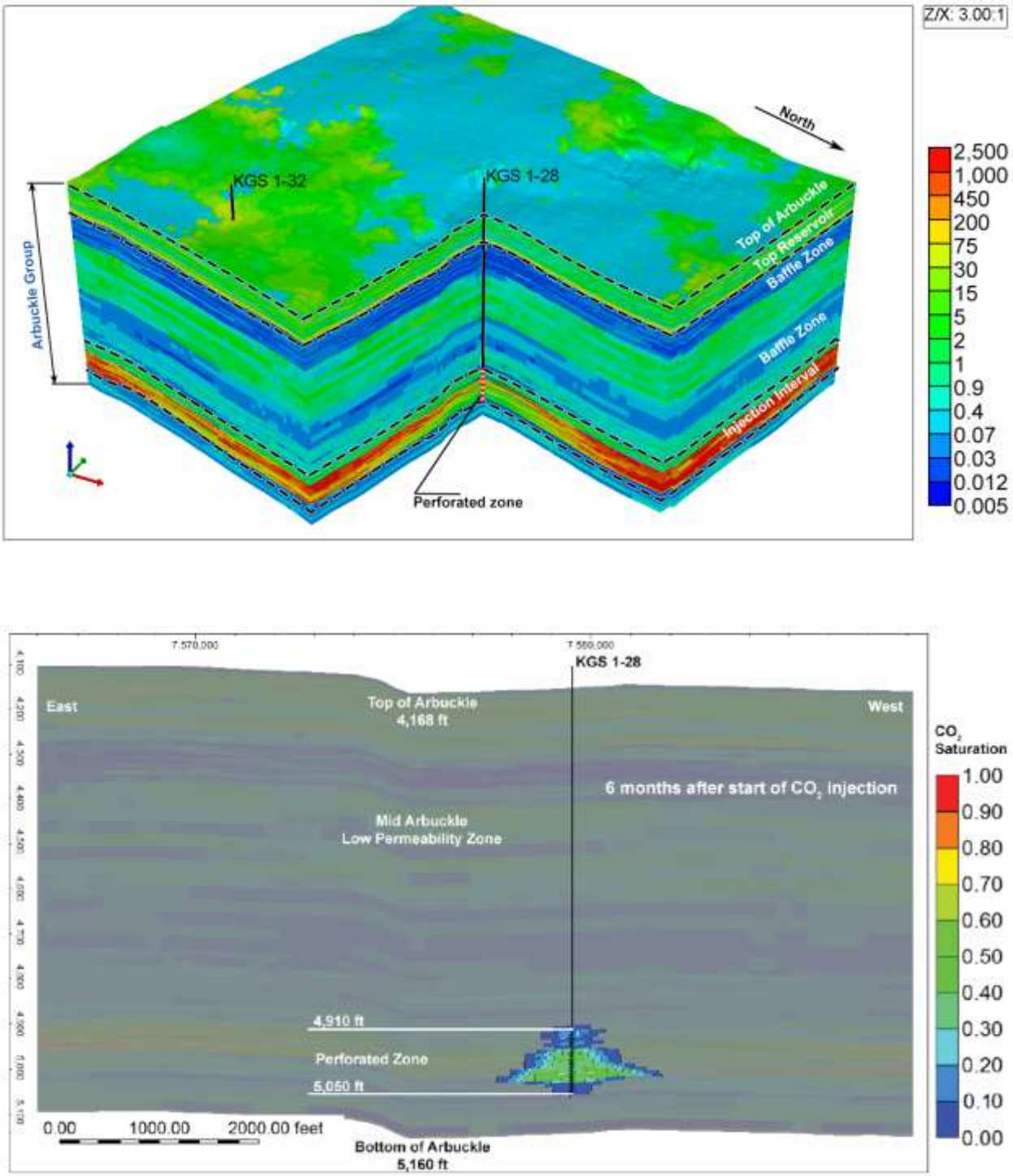

Figure 31 Horizontal permeability model of the Arbuckle Group derived using the Petrel geostatistical reservoir characterization software.

References

Amaefule, J.O., Altunbay, M., Tiab, D., 1993. Enhanced Reservoir Description: Using Core and Log Data to Identify Hydraulic (Flow) Units and Predict Permeability in Uncored Interval/Wells. Paper SPE 26436 presented at the SPE Annual Technical Conference, Houston, Texas, October 3-6.

Barker, R., Watney, W., Rush, J., Strazisar, B., Scheffer, A., Bhattacharya, S., Wreath, D., and Datta, S., 2012, Geochemical and mineralogical characterization of the Arbuckle aquifer: Studying mineral reactions and its implications for CO_2 sequestration, Master's thesis, Kansas State University, Manhattan Kansas**.**

Bhattacharya et al, 2003. Cost-effective integration of geologic and petropysical characterization with material balance and decline curve analysis to develop a 3D reservoir model for PC-based reservoir simulation to design a waterflood in a pure Mississippian carbonate field with limited log data: Kansas Geological Survey, Open-file Report 2003-31.

Chalbaud, C., Robin, M., Lombard, J., Martin, F., Egermann, P., and Bertin, H., 2009, Interfacial tension measurement and wettability evaluation for geologic CO_2 storage: Advances in Water Resources, v. 32, p. 98–109.

Dicker, A. I., and Smits, R. M., 1988, A practical approach for determining permeability from laboratory pressure-pulse decay measurements: Society of Petroleum Engineers, Conference Paper, International Meeting on Petroleum Engineering, November 1–4, 1988, Tianjin, China.

Fazalalavi, M., Fazalalavi, M., Fazalalavi, M., 2013. Determination of Reservoir Permeability Based on Irreducible Water Saturation and Porosity from Log Data and FZI (Flow Zone Indicator) from Core Data, International Petroleum Technology Conference, IPTC-17429-MS, Richardson, TX.

Kozeny, J., 1927. Sitzber. Akad.Wiss. Wien. Mth. Naturw. Klasse. 136, 271.

Loucks, R. G., 1999, Paleocave carbonate reservoirs: Origins, burial-depth modifications, spatial complexity, and reservoir implications: The American Association of Petroleum Geologists, Bulletin, v. 83, no. 11.

McIntosh, J., Walter, L., and Martini, A., 2004, Extensive microbial modification of formation water geochemistry: Case study from the midcontinent sedimentary basin, United States: Geological Society of America Bulletin, v. 116, no. 5–6, p. 743–759.

Scheffer, A., 2012, Geochemical and microbiological characterization of the Arbuckle saline aquifer, a potential CO_2 storage reservoir; Implications for hydraulic separation and caprock integrity: M.S. thesis, University of Kansas, Lawrence.

Volokin Y., Looyesttijn, W., Slijkerman, F., and Hofman, J., , 2001, A Practical Approach to Obtain Primary Drainage Capillary Pressure Curves from NMR Core and Log Data, Petrophysics, Vol. 42. No. 4; p. 334-343.

Watney, W.L., Guy, W.J., and Byrnes, A.P., 2001, Characterization of the Mississippian Osage Chat in South-Central Kansas: American Association of Petroleum Geologists Bulletin, v. 85, p. 85-114.

Whittemore, D. O., 2007, Fate and identification of oil-brine contamination in different hydrogeologic settings: Applied Geochemistry, v. 22, no. 10, p. 2,099–2,114.